nature communications

Article

https://doi.org/10.1038/s41467-025-62413-6

Gastrointestinal neuroprosthesis for motility and metabolic neuromodulation

Received: 27 June 2023

Accepted: 17 July 2025

Published online: 10 August 2025

Check for updates

Shriya Srinivasan[1,2,3,4,12], Marc-Joseph Antonini[5,6,7,12], Amro Alshareef[1,2,3], Atharva Sahasrabudhe[6,7,8], Josh Jenkins[1], Keiko Ishida[1,2,3], Johannes Kuosmanen[1,3], Alison Hayward[1,2,9], Seokkee Min[1,3], Robert Langer[1,3], Polina Anikeeva[6,7,8,10,11] ✉ & Giovanni Traverso[1,2] ✉

Gastrointestinal (GI) dysmotility and associated conditions affect over 20% of population, yet pharmacological, behavioural, and surgical interventions offer limited therapeutic efficacy. Targeted electrical stimulation addressing underlying neuromuscular pathology stands to transform our ability to treat dysmotility. Here, we developed a closed-loop GI neuroprosthesis which activates or relaxes GI tract musculature through electrochemical stimulation in response to sensed food stimuli. We additionally describe a tool supporting minimally invasive endoscopically guided implantation that can penetrate the mucosa, accurately localize the submucosa, and safely deploy this device to directly interface with the enteric nervous system. The neuroprosthesis enables generation of coordinated peristaltic waves, significantly increasing the motility rate in a swine model of oesophageal and stomach dysmotility ($p < 0.05$, student's t-test). Further, by directly modulating the myenteric plexus and thus mimicking meal ingestion, we induce peristalsis in a fasted state and achieve a metabolic response commensurate with a fed or satiated state. This neuroprosthesis and implantation platform expand opportunities in fundamental studies and treatments of metabolic and neuromuscular pathologies affecting the GI tract.

Gastrointestinal (GI) motility is orchestrated by multiple coordinating mechanisms, such as autonomic neural control (sympathetic and parasympathetic pathways) and ICC (interstitial cells of Cajal) that act as slow-wave pacemaker cells. Together, these mechanisms yield peristaltic waves that churn and propagate food through the GI tract[1]. Motility disorders of the oesophagus (gastroesophageal reflux disease (GERD), achalasia, and dysphagia) and stomach (functional dyspepsia, gastroparesis) affect more than a fifth of the population[2] and manifest in substantial morbidity, mortality, and economic burden[3,4]. While aetiologies range from diabetes and postsurgical complications to neural degeneration and hormonal imbalances, current pharmacological treatments are rarely targeted in mechanism or delivery[5]. Even

[1]Department of Mechanical Engineering, Massachusetts Institute of Technology, Cambridge, MA, USA. [2]Division of Gastroenterology, Hepatology and Endoscopy, Brigham and Women's Hospital, Harvard Medical School, Boston, MA, USA. [3]David H. Koch Institute for Integrative Cancer Research, Massachusetts Institute of Technology, Cambridge, MA, USA. [4]Society of Fellows, Harvard University, Cambridge, MA, USA. [5]Division of Health Sciences and Technology, Massachusetts Institute of Technology, Cambridge, MA, USA. [6]McGovern Institute for Brain Research, Massachusetts Institute of Technology, Cambridge, MA, USA. [7]Research Laboratory of Electronics, Massachusetts Institute of Technology, Cambridge, MA, USA. [8]Department of Chemistry, Massachusetts Institute of Technology, Cambridge, MA, USA. [9]Division of Comparative Medicine, Massachusetts Institute of Technology, Cambridge, MA, USA. [10]Department of Brain and Cognitive Sciences, Massachusetts Institute of Technology, Cambridge, MA, USA. [11]Department of Materials Science and Engineering, Massachusetts Institute of Technology, Cambridge, MA, USA. [12]These authors contributed equally: Shriya Srinivasan, Marc-Joseph Antonini. ✉e-mail: anikeeva@mit.edu; cgt20@mit.edu

with surgical intervention, restoration of peristalsis for conditions like achalasia, GERD, and gastroparesis remains inadequate[6,7]. Conspicuously, in 50% of GERD patients who receive fundoplication surgery following ineffective antisecretory pharmacotherapy, 62% require remedication after a decade[8]. In addition to its role in transporting food, motility also plays a key role in satiety. Following meal ingestion, gustatory secretions, oesophageal stretch[9], and gastric distension elicit afferent vagal signalling to the brainstem nuclei[10] regulating gastric motility[11], appetite, and satiety in a feed-forward manner[12]. Dysmotile GI organs lacking such physiological mechanotransduction and afferent signalling alter perceptions of satiety and hunger leading to detrimental behavioural consequences[13–15].

As an alternative to surgical and pharmacological intervention, electrical stimulation (ES) of the GI tract has been investigated since the 1960s, although few approaches have been successfully clinically translated and deployed as approved interventions[16,17] (Supplemental Table 1). Targeting the vagus nerve, the EnteroMedics Maestro VBLOC which consists of a cuff electrode wrapped around the vagus nerve (stainless steel lead encased in silicone, with platinum/iridium tip and ring stimulating electrodes; 2 ring and 2 tip electrodes), has been approved for obesity. Implanted in the serosa of the stomach, the Enterra (Enterra Medical; 2 platinum/iridium electrodes, 1 mm wide, with stainless steel lead encased in silicone rubber) gastric neurostimulator received FDA[18] approval under humanitarian device exemption for chronic, intractable nausea and vomiting due to gastroparesis, while the IntraPace abiliti (two bipolar pairs of sensing electrodes in fundus and stimulating electrodes in the vagal branch) have been received CE approval for obesity. Finally Medtronic's Interstim system targeting the sacral nerve (multi-ring electrode array) has been approved for the treatment of faecal incontinence[19]. Current ES devices, however, have shown inconsistent effect on gastric emptying[18,20,21]. This is likely because a single or few current sources producing constant pulse sequences may not be able to adequately replicate the spatial and temporal complexity of gastric signalling to restore function in a paretic state. Especially in pathologies affecting motility, the electrophysiological pathways underlying peristalsis may be affected. Thus, stimulation of a small group of cells may be inadequate to restore the natural signalling pathways responsible for peristalsis. Furthermore, GI peristalsis, like many processes involving the central and peripheral nervous system, is a closed-loop process, triggered by stimuli, such as temperature, irritants, and pressure in the oesophagus, as well as distension, nutrients, and chemical signalling in the stomach[22]. The open loop systems of current devices may contribute to their variable effects, misalignment with natural GI peristalsis, food intake, and neurochemical physiology, and in some cases create neural adaptation that renders stimulation less effective with time. Closed-loop systems for neural implants such as deep brain stimulators that sense epileptic seizures and respond with the appropriate stimulation are demonstrating significant advances over their open loop counterparts. Finally, despite a wide spectrum of parameters having been investigated for GI ES (ranging from 0.2 to 500 ms, 3 to 50 mA, 3 to 1670 Hz, and durations spanning from 30 minutes to 24 h), there is no consensus on conditions for triggering peristalsis (Supplemental Table 2)[16,23–27].

To coordinate peristalsis, it is likely advantageous to directly interface with the deep-set, distributed enteric plexi and circular muscle layers. However, this necessitates invasive surgery or advanced endoscopy methods. An example of such an advanced endoscopy method aiming at manipulating submucosal layers is the natural orifice transluminal endoscopic surgery (NOTES), which requires invasive dissection of the submucosal plane paired with continuous visualization. While promising, this recent technique has seen limited adoption by physicians as it requires specialized training.[28,29]. Altogether, there remains an unmet clinical need for an implantable device that can directly interface with the myenteric plexus and support closed-loop sensing and actuation to restore GI peristalsis.

Here, we describe an implantable GI neuroprosthesis which animates GI peristalsis via closed-loop, multichannel, electrical and chemical stimulation in response to sensed food stimuli. The neuroprosthesis features ES contacts longitudinally spaced at 1 cm intervals along the submucosal plane, mirroring the spatial arborization of distal myenteric nerve roots (Fig. 1a)[9].

We envision that a patient implanted with this device would undergo a period of monitoring to analyze their specific motility patterns. These data would then inform a customized sensing and actuation control paradigm using the device's multichannel contacts, which can be modularly adjusted based on the patient's needs. By interfacing directly with the ENS and muscularis, our device can bypass the disrupted signalling and directly stimulate the tissue to generate peristaltic contractions. In this study, we demonstrate the functionality of our device using seven channels, which provide greater spatial and temporal control of paralysed GI tissues compared to current implants. As we continue to refine our understanding of the spatiotemporal signalling dynamics in the oesophagus and stomach, our device is designed to scale to accommodate a higher number of channels, further enhancing its therapeutic potential.

To overcome challenges associated with submucosal implantation of a miniature neuroprosthesis, we design an endoscopic tool that enables anatomically precise, minimally invasive deployment of the neuroprosthesis (Fig. 1b). We demonstrate that this tool can precisely incise the mucosa, accurately identify, and dissect the submucosa, and safely implant the neuroprosthesis. Once implanted, we coupled the neuroprosthesis to a stimulation controller programmed to mimic physiological vagal efferent signalling[30] and generate coordinated peristalsis. We hypothesize that the neuroprosthesis will produce peristalsis in a paretic oesophagus or stomach in response to food stimuli (Fig. 1c). With the capability to mechanically actuate the organ, the neuroprosthesis can also induce artificial afferent mechanotransduction. By activating stretch-sensitive vagal afferents mimicking food ingestion in the fasted state, we hypothesize that neuroprosthetic stimulation will induce changes in satiety hormones that are commensurate with a fed state.

Results

Design and fabrication of GI neuroprosthesis

The neuroprosthesis was designed for effective electrical and chemical stimulation of oesophageal and gastric tissues, endoscopic delivery, and biocompatibility with submucosal tissues. The device form factor (1.25 ± 0.10 mm diameter) was chosen for deployment through the working channels of standard endoscopes (2.8–3.2 mm), while mechanical flexibility assured its resilience during endoscopic implantation and ability to form stable interfaces with the mobile GI tract (Fig. 1a). We studied the neuromuscular signalling patterns which give rise to peristaltic activity ex vivo to recapitulate them with the neuroprosthesis (Methods); sequential activation of myenteric branches in the muscularis elicited peristalsis of the arborized muscle segments in both circular and longitudinal muscle layers, which synergize for peristaltic movements[9]. These informed spacing and placement of the neuroprosthesis in the submucosal layer on top of the muscularis.

To create a multimodal neuroprosthesis, we applied a fibre drawing process recently adapted for fabricating multifunctional neural probes[31–34]. During fibre drawing the macroscale template of the neuroprosthesis was transformed into the mm-scale fibre through application of controlled heat and stress (Fig. 2a–c). The final design included 7 electrodes composed of stainless steel, commonly used to deliver ES in laboratory, surrounding a microfluidic drug delivery channel within a polycarbonate cladding, chosen for its biocompatibility. To integrate high-melting temperature (T_m) stainless steel

electrodes into the polycarbonate cladding with significantly lower glass transition temperature we leveraged a material convergence technique[32]. Stainless steel was selected as the electrode material due to its biocompatibility, robustness, wide accessibility, cost-effectiveness, and ease of integration into implantable devices. The electrodes were subsequently exposed along the fibre surface through laser etching of the polymer cladding. The electrochemical surface area at the electrode-tissue interface was optimized to maximize current injection and reduce impedance (see Methods, Supplemental Fig. 1). To insulate the stainless-steel electrodes at the tip of the device, 5-min epoxy (DevCon) was applied to the electrodes while avoiding the lumen of the microfluidic channel.

Note, that while stainless steel was chosen for these practical reasons, alternative materials with higher charge injection capacity, such as platinum, iridium oxide, or carbon nanotube yarn, can be straightforwardly implemented to enhance performance and clinical utility of the device. Additionally, coatings and electrochemically deposited materials can be considered for further improving the electrochemical properties of the electrodes in subsequent iteration of this work.

To characterize the electrical and electrochemical properties of the stimulating electrodes exposed by laser etching, we first performed electrical impedance spectroscopy. The areal impedance values recorded at 100 Hz, 1 kHz and 10 kHz were 4.95 ± 1.04 kΩ/mm^2, 1.20 ± 0.22 kΩ/mm^2, 0.51 ± 0.08 kΩ/mm^2, respectively (Fig. 2d). Using cyclic voltammetry at a slow sweep rate of 20 mV/s[35] we estimated the water-stability window between potentials of +1.37 and −1.25 V vs. Ag/AgCl, which mark the onsets of oxygen evolution reaction (OER) and hydrogen evolution reaction (HER), respectively (Fig. 2e). Charge injection capacity (CIC) of the electrodes was then determined based on voltage transients in response to biphasic, symmetric rectangular current pulses (half-phase period = 100 μsec, interphase delay = 33.3 μsec) ranging in amplitude between 0.5–10 mA (Fig. 2f, g). Since the onset of HER (1e$^-$ transfer reaction) was found to be lower than that for OER (4e$^-$ transfer reaction), the former potential limit was used to calculate the CIC values. To assess the stability of the electrode, we measured the maximum cathodic potential (E_{mc}) defined as the most negative polarization across the electrode-electrolyte interface[36,37]. The E_{mc} of stainless-steel electrodes was below the water reduction potential of −1.25 V for current amplitude ≤10 mA (Fig. 2g, and Supplemental Figure 2a) suggesting safe use of these electrodes at these amplitudes. We additionally conducted accelerated aging tests of the neuroprosthesis in phosphate buffered saline (PBS) by applying 144 × 10^6 biphasic pulses with 4 mA, the target stimulation amplitude of 2 mA with a safety factor of two. The maximum cathodic potential (E_{mc}) measured after 9 M, 18 M, 36 M, 54 M, 72 M, 90 M, and 144 M pulses remained below the water reduction potential of −1.25 V indicating long-term stability of the electrodes (Supplemental Figure 2b–c). We observed a slight increase of the absolute value of the E_{mc} after 144 M pulses; which corresponds to approximately 8 years of use, assuming 58.6 voluntary swallowing events per meal[38], one spontaneous swallowing per

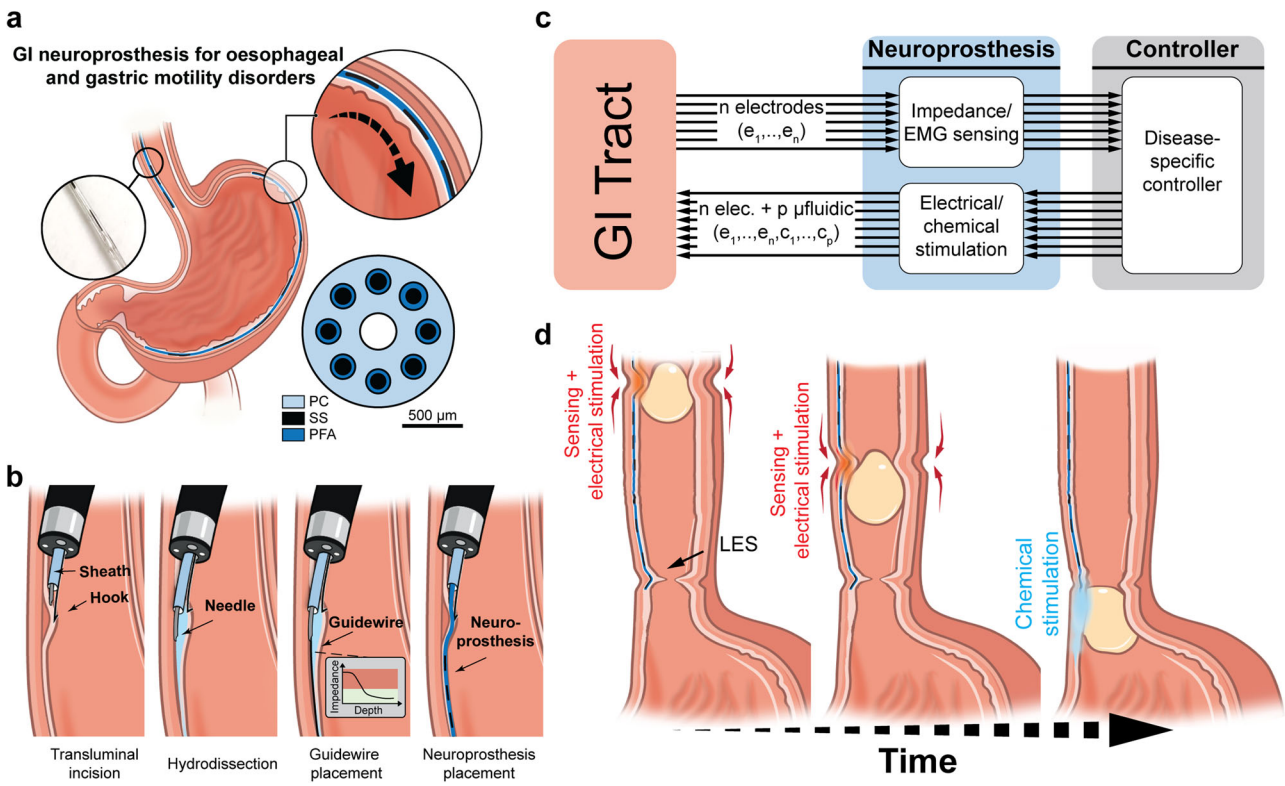

Fig. 1 | Closed-loop gastrointestinal neuroprosthesis and minimally invasive submucosal implantation tool. a The neuroprosthesis augments oesophageal and gastric motility through multichannel electrical and chemical stimulation. Insets demonstrate patterned electrode contacts which mimics physiological signalling and the cross section, dimensions, and layout of the implant. **b** The submucosal implantation tool facilitates minimally invasive and precise implantation through the following steps: (1) The sheath is passed through an endoscopic channel. While the self-expanding nitinol hook pulls counter tension on the luminal wall, the penetrating needle incises the lumen and advances until the submucosa is localized based on tissue impedance; (2) Hydrodissection separates the submucosa from the muscularis; (3) A guidewire is advanced to dissect the plane along the curvature of the organ and ensure accurate localization through impedance measurement. 4) The neuroprosthesis is inserted into the submucosal space. **c** Schematic (top) outlines the system design wherein closed-loop sensing and actuation is performed. **d** Upon sensing a bolus of food (peach), programmed patterns of ES (red) and/or chemical stimulation (blue) contract and inhibit the neuromusculature appropriately to recreate peristalsis. Graphical representations in b and d are not to scale. PC: Polycarbonate, SS: Stainless steel, PFA: Perfluoro alkoxy alkanes, EMG: Electromyography, LES: Lower oesophageal sphincter. We thank Virginia Fulford for her contributions to the illustration of this figure.

https://doi.org/10.1038/s41467-025-62413-6

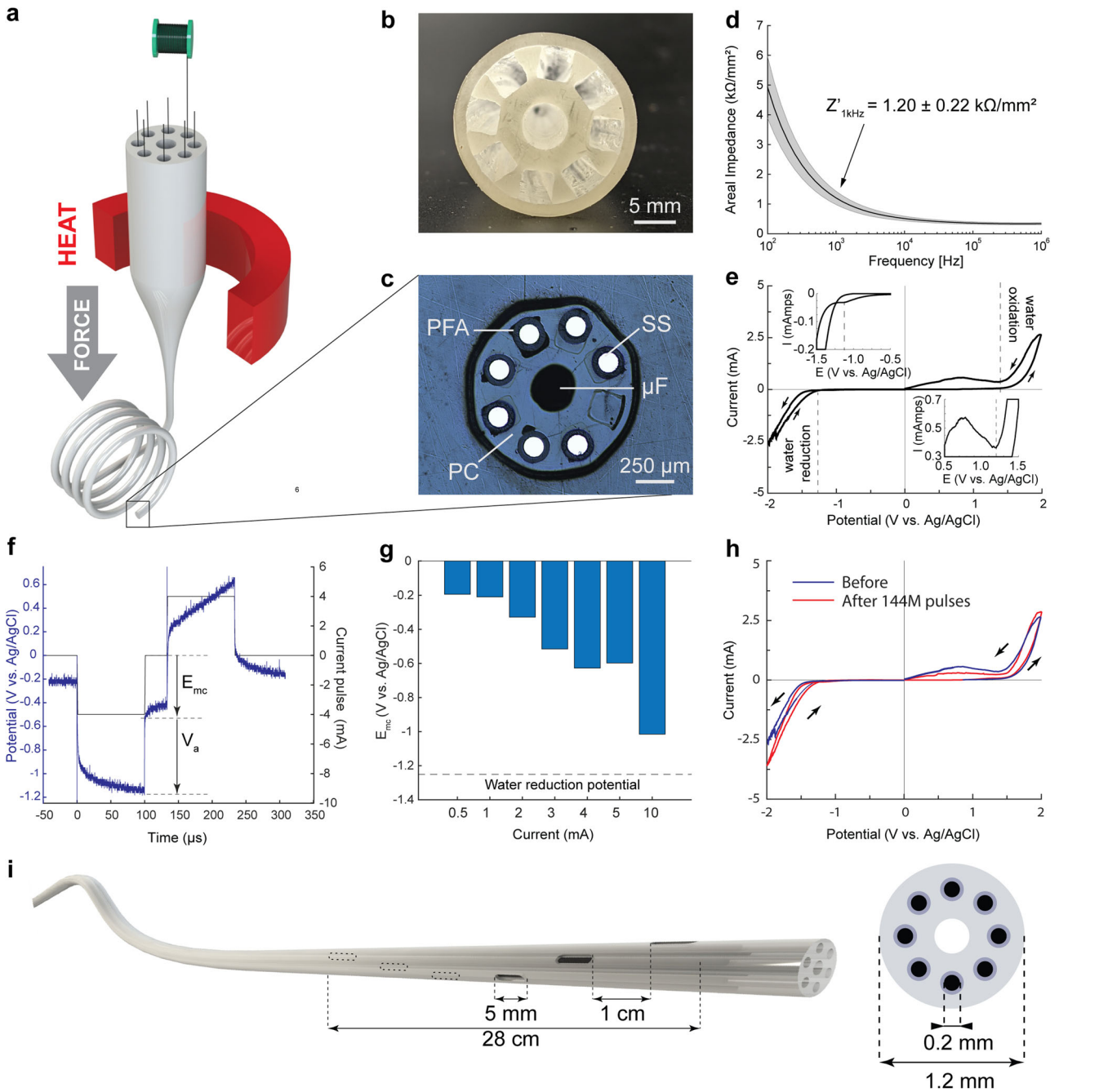

Fig. 2 | Fabrication and characterization of the closed-loop gastrointestinal neuroprosthesis. a–c Schematic of the thermal drawing process (**a**) during which a macroscopic preform (**b**) is heated and stretched into a (**c**) mm-scale device. During this process, stainless steel microelectrodes are fed into the preform and embedded into the final device. **d** Electrochemical impedance spectrum of the 0.2 mm × 5 mm stainless-steel electrodes. (1 device, 7 electrodes, shaded area represent the standard error of the mean), **e** Cyclic voltammogram of the stainless-steel electrodes in phosphate buffered saline (PBS). **f** Representative potential transient response to a ± 4 mA symmetric, biphasic current pulse of 100 μsec half-phase period and a 33.3 μsec interphase delay, and estimation of the maximum cathodic potential E_{mc}. **g** E_{mc} of the electrode following 0.5, 1, 2, 3, 4, 5, and 10 mA current pulses. **h** Accelerated aging of the electrode: Cyclic voltammogram before and after the accelerated aging experiment (144 M pulses). **i** Schematic representation of the final form of the neuroprosthesis, highlighting the length and the spacing of the exposed electrodes. PC: Polycarbonate, SS: Stainless steel, PFA: Perfluoro alkoxy alkanes, μF: microfluidic channel, Ag: Silver, AgCl: Silver Chloride.

minute while awake, and three swallowing events per hour while asleep[39], each assisted by the neuroprosthetic stimulation. Additionally, a cyclic voltammogram collected following the accelerated aging of the electrodes confirmed their stability at 4 mA current amplitude (Fig. 2h). Note, that accelerated aging tests in PBS may not fully replicate physiological conditions. To evaluate the impact of repeated mechanical deformation during peristalsis on the electrodes, we measured the electrical impedance and E_{mc} (2 mA current) following 1, 10, 100, 1000, and 10000 buckling cycles (10 cm long fibre, 5 mm displacement, 1 cm/sec). The impedance value varied between 3 + /− 1 kΩ while the E_{mc} remained below the water reduction potential of −1.25 V, demonstrating that the electrodes were not significantly affected by the repeated deformation (Supplemental Figure 2d, e). Further, to evaluate the changes in electrochemical properties during mechanical deformation (peristalsis), we performed electrical impedance spectroscopy and cyclic voltammetry at a sweep rate of 100 mV/s between 1 V and −1.2 V vs. Ag/AgCl at rest and when the fibre was bent (10 cm long fibre, clamped, 5 mm

longitudinal displacement). The areal impedance value and the CV curves were not substantially affected by the mechanical deformation (Supplementary Fig. 2 f–h) Finally, we characterized the mechanical properties of our neuroprosthesis. The neuroprosthesis exhibited bending stiffness values between 516-645 N/m over the frequency range of mammalian locomotion, respiration, and heartbeat (Supplemental Fig. 3). The tensile behaviour of the neuroprosthesis in the elastic regime was dominated by the properties of polycarbonate with a Young's modulus $E = 10.1 \pm 0.66$ GPa ($n = 3$) ($E_{Polycarbonate}$ = 2.2 GPa, E_{Steel} = 200 GPa). The hollow core of the miniature neuroprosthesis contributed to its substantially reduced flexural modulus $E_f = 400.0 \pm 15.0$ MPa ($n = 3$) as compared to the flexural modulus of a solid polycarbonate beam (2.3 GPa). Comparatively, most electrodes made for deep brain stimulation (DBS) consist of platinum–iridium wires encased in a polyurethane sheath[40], and typically have a Young's moduli in the range of 10–1000 MPa dominated by the properties of polyurethane[41].

Design and validation of submucosal implantation tool

A minimally invasive submucosal implantation tool was designed with the considerations of endoscopic incision, anatomic localization, dissection, surgical risk mitigation, and precision control availed at a length of two meters through the 2.8–3.8 mm working channels of standard endoscopes[42] (Fig. 1c, and Supplemental Fig. 4, and Methods).

Given the shallow angle of attack for endoscopic incision, a needle profile capable of low-force incision of the distensible mucosa without slipping is required to prevent trauma or perforation. Building on prior optimization of needle tips (Methods)[43], we evaluated the following geometries: triple grooved tip, pitchfork shape, standard bevel (25 g and 19 g), curved tip, broad base, and dual point (Fig. 3a, and Supplemental Fig. 5) with and without a self-expanding nitinol hook which applies a stabilizing counter force. For all geometries, 20° angle of attack on porcine stomach and oesophageal tissues resulted in higher forces as compared to 90° (Fig. 3b, $p < 0.05$, student's t-test, $n = 5$ trials). At 20° angle, the curved design with the nitinol hook provided the greatest reduction in force as compared to standard 19- and 26-gauge needles ($p < 0.05$, student's t-test, $n = 5$ trials) and was selected for the submucosal implantation tool. In vivo, the tool's incision in the oesophagus and stomach measured 1.8 ± 0.3 mm and 2.12 ± 0.12 mm ($n = 3$ each), respectively. No stretching, sliding, or tearing of tissue were observed.

While visualizing the stomach using laparoscopic ultrasound, the tool's needle was endoscopically introduced into the lumen and sequentially advanced through each layer to the peritoneum, while monitoring impedance and position (Fig. 3c–f). Each impedance recording was performed at 1 kHz and required 1-2 seconds of stable positioning.

We found that the impedance as measured by the nitinol guidewire values in the submucosa and muscle layers were two orders of magnitude lower than the lumen, mucosa, serosa, and peritoneum (Fig. 3g, $n = 6$ per anatomic location in the one animal, $p < 0.01$, student's two-tailed heteroscedastic t-test), enabling localization of the submucosal layer. Hydrodissection with saline was performed to separate planes, and the device was inserted into the submucosal space. Following insertion saline was suctioned, collapsing the muscularis propria and the mucosa layer around the prosthesis. The submucosal implantation tool accurately localized and enabled dissection of the submucosal plane following the natural curvature of the oesophagus and stomach ex vivo ($n = 7$) and in vivo ($n = 4$) without perforation, haemorrhage, haematoma, blood loss, or gross tissue trauma (Fig. 3h, i and Supplemental Fig. 6). Histological tissue analyses corroborated accurate identification of the desired plane and effective separation of muscularis planes and revealed no unanticipated tissue damage (Fig. 3j, k). Methylene blue dye injected during hydrodissection and histological indicator stains were identified exclusively in the targeted locations. The main endoscopic stages of 1) localization & dissection, 2) implantation and 3) closure are shown in Fig. 3l–n.

Our tool overcomes key limitations of previously reported approaches such as NOTES, including postoperative recovery, and complexity and cost of implementation[44]. Furthermore, the ability to accurately localize and safely hydrodissect the submucosa using a single tool and a working channel of an endoscope creates new opportunities for submucosal implants.

Design of closed-loop controller and optimization of stimulation and sensing parameters

To mimic physiological peristalsis, we designed a trigger-based controller that executes an ES pattern to active neuromusculature in a coordinated fashion upon sensing a bolus of food in the oesophagus (Fig. 4a, and Supplemental Code 1). System operation comprises three stages. (1) A bolus of food is detected by measuring the impedance value at the proximal electrode, which is used as a proxy for mechanical force applied at that electrode. (2) After the impedance value crosses a set threshold, an electrical stimulation pattern is triggered, based on parameters optimized in in vivo and ex vivo models. The peristaltic wave begins at the first electrode and then propagates to each subsequent electrode with a time delay of 1 s until it reaches the most distal electrode. (3) Following the termination of the stimulation train, a 5 second refractory period is enforced to mimic natural deglutitive inhibition. After the refractory period, if a bolus of food (the same or the subsequent one) is detected at electrode 1, the cycle begins anew and another peristaltic wave is initiated. The controller's stimulation parameters (Supplemental Table 3) can be tailored to a specific disease and patient physiology. We applied our controller in a model of induced functional oesophageal paresis and depressed gastric motility (Methods). ES stimulation parameters were optimized through a comparative characterization of peristaltic dynamics using in vivo and ex vivo models using commercial electrodes. For the oesophagus, stimulation parameters spanning commonly reported values from literature were evaluated (frequency: 20, 40, 100 Hz | peak-to-peak amplitude: 1, 2, 3, 4, 6, 8 mA | pulse train length: 0.5, 1, 3 s | n = 4 animals | 10 repetitions of each condition, Fig. 4b–e, and Supplemental Table 2). Neural activation was expected at pulse widths of 100 μs while longer widths were anticipated to activate muscle directly[16]. Image analysis enabled a calculation of the percentage of closure in the oesophageal lumen (Fig. 4f–g). At a 40 Hz 1 s pulse trains, 2 mA, 100 μs pulse width yielded complete oesophageal closure, with higher amplitudes leading to fractional closure due to muscle fatigue or hypertonicity (Fig. 4b). Utilizing a 2-mA amplitude and 0.5 s pulse train, a frequency sweep revealed that 40 Hz stimulation produced sustained oesophageal contraction with $89 \pm 4\%$ closure (Fig. 4c). At 2 mA and 40 Hz, a sweep of pulse train lengths revealed no significant difference between conditions (Fig. 4d, $p < 0.05$, student's t-test, n = 4 animals). Thus, 40 Hz, 2 mA and 100μs pulse width, 0.5 s pulse duration, which enabled complete, repeatable, oesophageal closure were selected for the closed-loop controller for oesophageal hypomotility (Supplemental Table 4). EMG graded monotonically with stimulation amplitude (Fig. 4e between 0.25–4.0 mA, availing a linear stimulation-response relationship for controller optimization. Ex vivo, point source stimulation activated neuromusculature 7.2 ± 4.5 mm proximally and distally ($n = 35$ trials) motivating 10 mm electrode spacing on the neuroprosthesis. Electrically stimulated segments relaxed (full opening) 1.7 ± 0.3 s following the end of the pulse trains. Thus, oesophageal ES was programmed to repeat at 1 s intervals consistent with normal swallowing dynamics characterized by temporal overlap in the distal and proximal segment contraction mitigating reverse propagation[45].

https://doi.org/10.1038/s41467-025-62413-6

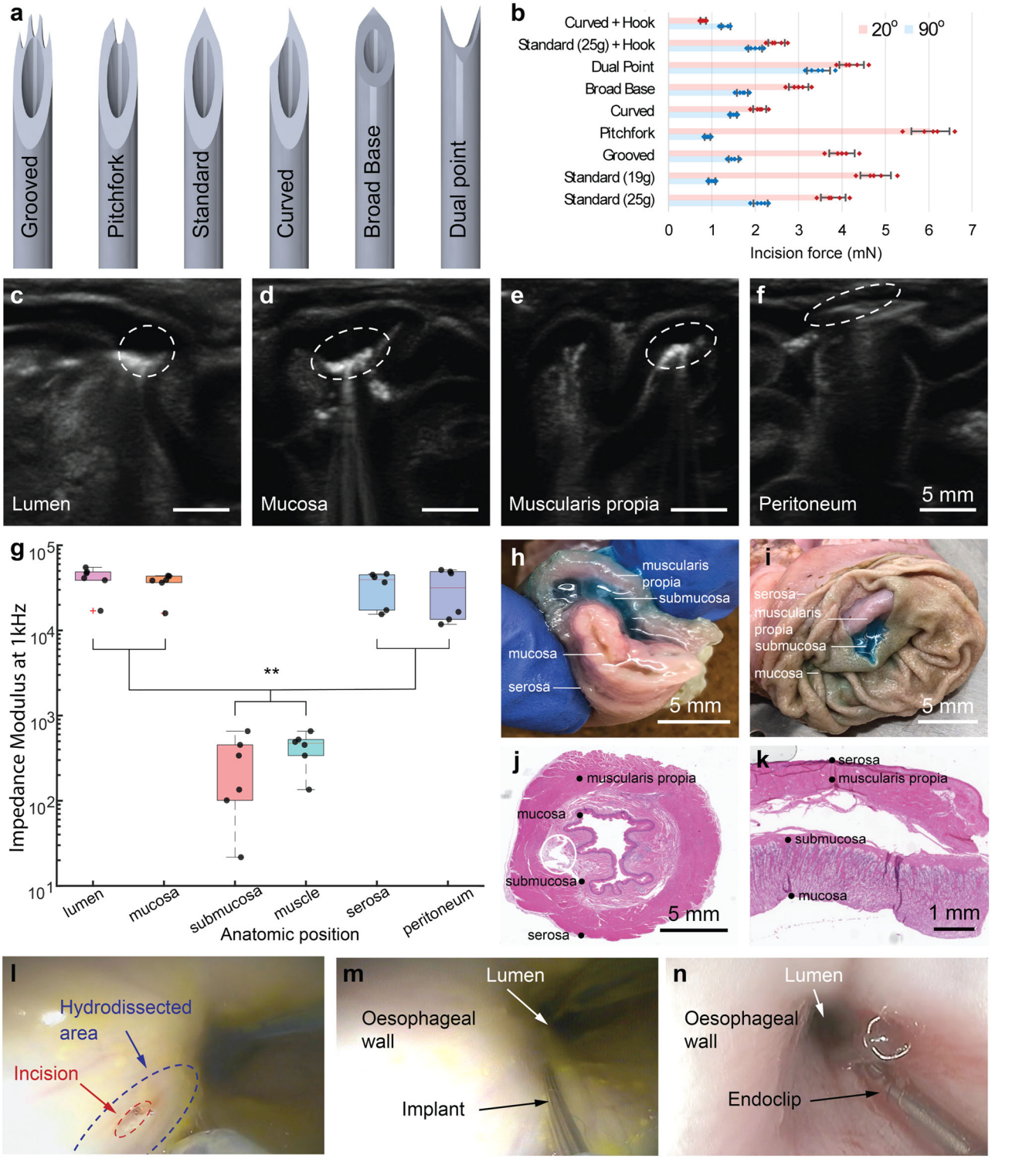

Fig. 3 | Safety and efficacy testing of submucosal implantation tool. a Needle geometries designed to minimize penetration force during endoscopic intraluminal approach. **b**, Force of penetration was significantly increased at 20 degrees as compared to a 90° of attack ($p < 0.05$, student's two-tailed heteroscedastic t-test, $n = 5$ trials, mean and standard deviations are plotted). The curved design with a hook demonstrated the lowest penetrating force ($p = 5 \times 10^{-20}$, $n = 5$ trials). Impedances were recorded as the needle advanced through the (**c**) lumen (**d**) mucosa (**e**) muscularis propria and (**f**) peritoneum. **g** The impedance of the submucosa and muscularis were significantly different from other layers, enable precise localization (**$p < 0.001$, submucosa and muscularis v other layers: $p = 2 \times 10^{-10}$, Student's two tailed heteroscedastic t-test, $n = 6$ measurements in one animal). Box plot indicates the minima, maxima, and median, first and third quartile, with individual measurements as black points. **h**–**k** Injection of methylene blue saline enabled accurate dissection of the submucosal layer as seen in gross images and histology of the (**h**, **j**) oesophagus and (**i**, **k**) stomach. This was performed in 3 animals. **l**–**n** Endoscopic visualization aided the (**l**) incision, (**m**) implantation, and (**n**) closure with one resolution clip.

https://doi.org/10.1038/s41467-025-62413-6

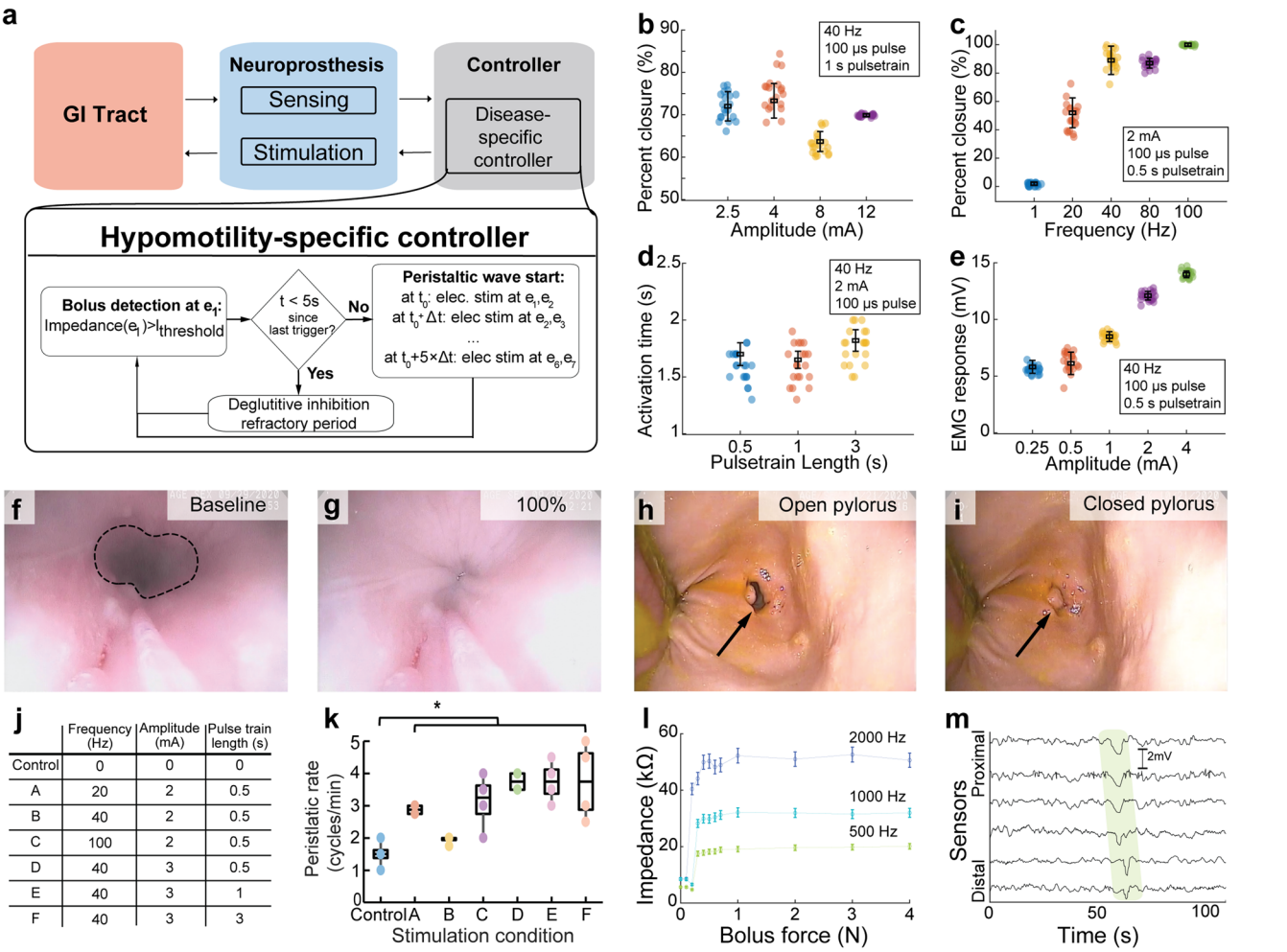

	Frequency (Hz)	Amplitude (mA)	Pulse train length (s)
Control	0	0	0
A	20	2	0.5
B	40	2	0.5
C	100	2	0.5
D	40	3	0.5
E	40	3	1
F	40	3	3

Fig. 4 | Optimization of Electrical Stimulation for Oesophageal and Gastric Motility. a Disease-specific controller scheme of the myenteric neuroprosthesis highlighting the proof-of-concept model for hypomotility. **b**–**e** The ES parameters of (**b**) amplitude, (**c**) frequency and (**d**) pulse train length were optimized for oesophageal contraction time using ex vivo and in vivo models. ($n = 4$ animals | 10 repetitions of each condition, mean and standard deviations are plotted) **e** An amplitude sweep of the ES parameters (with a set frequency of 40 Hz, and pulse train length of 0.5 s) elicited a monotonically increasing electromyographic (EMG) responses in the smooth muscle. ($n = 4$ animals | 10 repetitions of each condition, mean and standard deviations are plotted) **f, g** Endoscopic views of the oesophagus during titration of muscle activation and contraction duration enabling graded control of closure. Endoscopic visualization of the opening (**h**) and (**i**) closing of the pylorus was utilized to characterize gastric peristalsis. **j** Panel of ES parameters evaluated for stomach motility. **k** All stimulation conditions yielded an increase in peristaltic rate (pyloric cycles/time), with setting C optimizing activity with minimal energy. Mean and standard deviations are plotted. (* $p < 0.01$, $p <= 0.001$, student's two-sided t-test, $n = 4$ animals) **l** Changes in impedances at 500 Hz (green), 1000 Hz (blue), and 2000 Hz (purple) of proximal electrodes of the neuroprosthesis implanted in the swine oesophagus enable detection of ingested boluses, applying forces greater than 0.2 N. ($n = 3$ samples, 11 repetitions- mean and standard deviations are plotted) **m** EMG signals recorded from implanted neuroprosthesis can be used to monitor the peristaltic waves.

Using an optimization strategy analogous to that for oesophageal ES, parameters for gastric motility were optimized through a comparison of the rate of pyloric closure (Fig. 4h, i), which is proportional to peristaltic activity in the fasted state[46,47] in response to six sets of parameters (Fig. 4j). All ES conditions, excluding set B, produced a significant increase in peristaltic rate as compared to the baseline control ($p < 0.01$, student's t-test, Fig. 4k, $n = 4$ animals). Stimulation settings in A (20 Hz, 2 mA and 100µs pulse width, 0.5 s pulse duration) were chosen for implementation in the neuroprosthesis as they provided a significant increase with the most minimal intervention.

To perform closed-loop stimulation, the prosthesis detects food stimuli to initiate peristalsis. This feedback component of the closed-loop controller is performed by the proximal electrodes using differential amplification of the impedance measured at 0.5, 1, and 2 kHz frequencies (Fig. 4l). A significant increase in the impedance is observed at forces greater than 0.2 N, which correspond to the pressures exerted by semi-solid and solid foods[48,49]. Additionally, muscle activation recorded via electromyography (EMG) can also be used to detect ingestion, initiate peristalsis, or inform the amplitude of stimulation to produce coordinated peristalsis (Fig. 4m).

Neuroprosthetic augmentation of motility

Following controller optimization, the neuroprosthesis was implanted in the oesophagus of a swine model of depressed motility ($n = 3$) and its function was assessed via endoscopy, fluoroscopy, and functional lumen imaging. Functional lumen imaging using impedance planimetry has become a standard of care for assessing oesophageal motility and provides the most quantitative metric in the swine model. No significant differences were found between pre- and post-implantation distensibility index, minimum cross-sectional area (CSA_{min}), or pressure at baseline (8.2–9.4 mmHg at 20 mL inflation), indicating that the neuroprosthesis itself did not adversely affect the baseline properties of the oesophagus ($p < 0.05$, $n = 6$ trials, paired t-test). The neuroprosthesis effectively generated swallowing movements with duration, sequence, and axial pressures insignificantly

https://doi.org/10.1038/s41467-025-62413-6

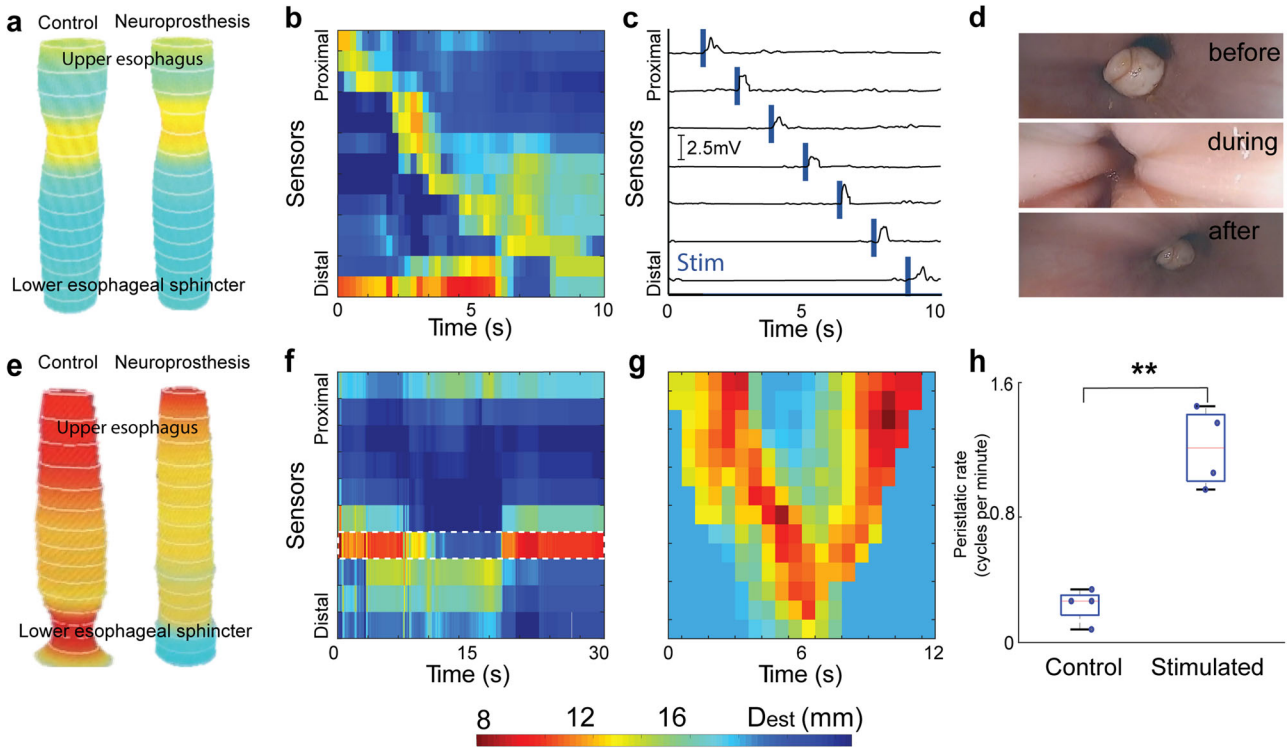

Fig. 5 | Neuroprosthetic generation of peristalsis. a Functional lumen imaging data from the Endoflip device of the oesophagus during reflex- and neuroprosthetically-initiated swallows demonstrates similarity in contraction strength and shape. **b** Neuroprosthetically initiated peristalsis in the oesophagus reveals a coordinated swallowing pattern, including relaxation of the lower oesophageal sphincter (LES) (distal) in response to microfluidic glucagon infusion. **c** Filtered and rectified EMG signal recorded at each electrode during neuroprosthesis-initiated peristalsis in the oesophagus elucidates a propagative sequence in response to sequential stimulation pulses at each electrode (blue). **d** Endoscopic visualization of the bolus before (top), during (middle) and after (bottom) neuroprosthetic contraction of the oesophageal muscle for bolus propagation. **e** Neuroprosthetic glucagon infusion yields relaxation (right) of the tonic LES (left) as visualized with intraluminal imaging from the Endoflip device. **f** Reversible relaxation of the LES induced by glucagon infusion occurring from ~t = 11 – 19 seconds. **g** Representative functional luminal imaging during antero- and retrograde peristalsis demonstrates the versatile programmability of the controller. **h** Stomach motility was significantly increased by neuroprosthetic stimulation (**$p = 0.001$, student's two-tailed heteroscedastic t-test) as compared to the control in a model of hypomotility. Box plot indicates the minima, maxima, and median, first and third quartile, with individual measurements as black points cpm: cycles per minute. Dest = estimated luminal diameter. Mean and standard deviation are plotted.

different from those of natural swallows[8] in control conditions ($p < 0.05$, paired t-test, $n = 30$ trials (10 per animal), Fig. 5a). Inflation of the intraluminal manometer to 20 mL manifested in forces and the corresponding changes in electrode impedance above the sensing threshold of the neuroprosthesis', triggering sequential stimulation yielding a peristaltic wave as measured by functional lumen imaging (impedance planimetry) and EMG (Fig. 5b, c). To test the efficacy of the neuroprosthesis in propelling food, radio-opaque boluses of barium sulphate (see "Methods") were placed in the proximal oesophagus, triggering activation along the neuroprosthesis which propelled the bolus down the oesophagus (Fig. 5d, and Supplemental Figure 7). These results demonstrate that the neuroprosthesis can be used to induce peristalsis in hypomotile conditions and effectively propel food in a paretic oesophagus.

In addition to demonstrating peristalsis in a model of hypomotility, we leveraged the neuroprosthesis' microfluidic channel to release inhibitory compounds facilitating relaxation of hypertonic musculature for conditions such as achalasia and spastic oesophagus. The neuroprosthesis' distal tip was implanted in the lower oesophageal sphincter and glucagon[50], a known smooth muscle relaxant used in the GI tract, genitourinary, and cardiovascular systems[50], was infused through the microfluidic channel. This chemical stimulation yielded relaxation of the sphincter within 10-20 s. Average luminal distensibility substantially increased from 6.8 ± 1.2 mmHg to 15.8 ± 1.7 mmHg (Fig. 5e-f). Muscle tone after relaxation returned to baseline within 1.5 minutes whereupon repeated infusions led to relaxation. In contrast, injection of saline control produced no measurable effect.

To further validate the long-term efficacy of the neuroprosthesis, we investigated whether our platform was capable of eliciting repeated actuation without inducing muscle fatigue, a known adverse effect of ES[51]. We performed continuous stimulation for 160 seconds, which is substantially longer than relevant therapeutic applications, and observed less than 10% reduction in force production (Supplemental Figure 8). This minimal fatigue induction is likely due to our selection of the lowest effective stimulation parameters (amplitude, frequency, and duration) to achieve peristalsis, preventing unnecessary overexcitation and muscle fatigue. The neuroprosthesis can be programmed to meet the actuation requirements of varied dysmotility by adjusting the timing, spacing, refractory period, strength of contraction, and sequence of activation. As a proof of concept, we programmed the controller to elicit anterograde and retrograde peristaltic waves (Fig. 5g) and demonstrated the capability of the neuroprosthesis to carry out this pattern in the oesophagus.

Finally, to assess its ability to drive gastric motility, the neuroprosthesis was implanted in the antrum or cardia of the stomach using the submucosal implantation tool. Under deep anaesthesia when no spontaneous peristaltic waves were observed and the pyloric closure rate had dropped below once per min, 0.5 s pulse trains of 20 Hz stimulation spaced 3 s apart on consecutive electrodes were applied. A two-fold increase in the peristaltic rate was observed over a 20-minute period (Fig. 5h, $p < 0.05$, paired t-test, n = 4 animals). In all trials, the

https://doi.org/10.1038/s41467-025-62413-6

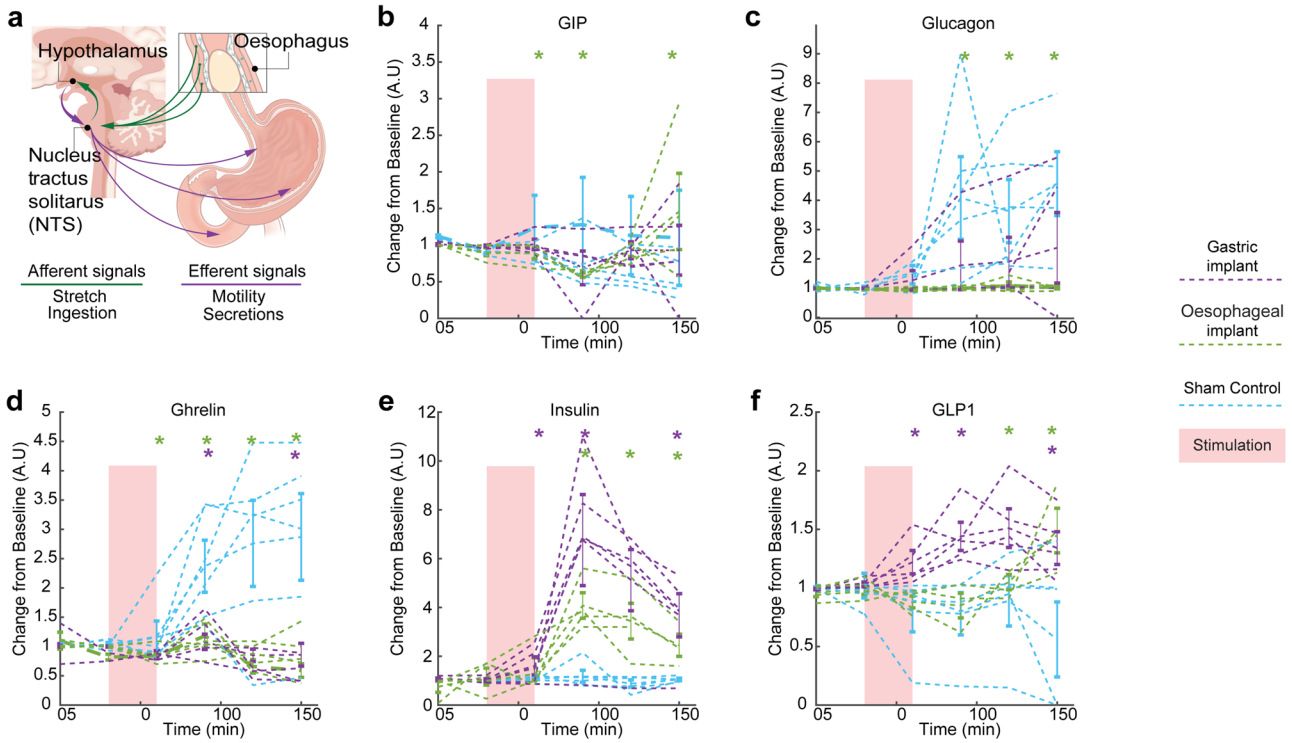

Fig. 6 | Neuromodulation of oesophageal vagal afferents yields illusory metabolic satiety. a Mechanotransducers in the stomach and oesophagus relay afferents to the NTS and DMN which regulate metabolic hormones and satiety. **b–f** Response of hormones in the blood to stimulation between minute 30-60 normalized to their baseline levels in animals with no stimulation (control, blue), oesophageal (green), and gastric (purple) stimulation ($n = 5$ animals). GIP: Gastric inhibitory polypeptide, GLP-1: Glucagon-like peptide-1. Error bars indicate the standard deviations around the means. Stars indicate $p < 0.05$ as per a 2-tailed heteroscedastic t-test comparing the experimental (gastric or oesophageal) stimulation to the no stimulation group.

neuroprosthesis complied with the tissue movement, exhibiting no sliding, protrusion, or impediment to normal peristalsis. These results suggest that the neuroprosthesis can be used to artificially generate peristalsis and increase gastric motility.

Metabolic neuromodulation

When implanted in the oesophagus, the neuroprosthesis resides alongside primary sensory and low-threshold mechanoreceptors innervating the thoracic oesophagus which originate from the nucleus tractus solitarius (NTS) and dorsal motor nucleus (DMN) in the brainstem. In the stomach, antral placement was performed to maximize contact with stretch receptors which relay afferents to the NTS[13,15]. The NTS and DMN relay sensed information to the hypothalamic neurons, which integrate ingestion, hunger, and satiety signals[52], in turn, efferently controlling hormonal secretion and motility (Fig. 6a). We sought to explore the effect on satiety of stimulating vagal afferent signalling through mimicking ingestion and gastric peristalsis. To mimic peristalsis following ingestion, we implanted the neuroprosthesis in 5 animals that were fasted overnight and performed 30 min of sequential stimulation (oesophagus: 40 Hz, 2.5 mA, 100 μs, and 0.5 s; stomach: 20 Hz, 2 mA, 0.5 s) with 30 s rest periods separating 120 s stimulation epochs to mitigate fatigue. Satiety and disorders thereof are profiled by measuring levels of the metabolic hormones, such as glucagon-like peptide-1 (GLP-1), insulin, glucagon, gastric inhibitory polypeptide (GIP), and ghrelin that fluctuates with hunger and satiety. Therefore, to characterize the effect of the neuroprosthesis on the body's satiety response, metabolic hormone levels in the blood were measured at 0, 15, 30, 45, 60, 90, 150 minutes, with stimulation occurring between 30-60 minutes. Raw and normalized data is provided in Supplementary Data 1. Another group of 5 animals served as the control group. Since animals are fasted overnight, the response from the control group is approximately stable except for ghrelin and glucagon which are secreted to compensate for the building hunger. Oesophageal actuation in the fasted state resulted in a significant increase in GLP-1 and insulin levels along with a moderate suppression of ghrelin and no change in glucagon in the response phase compared to the baseline – commensurate with a fed state[53] ($p < 0.05$, student's t-test, Fig. 6b–f). GIP initially decreased, but then increased beyond control levels. Gastric actuation resulted in a significant increase in GLP-1, insulin, and glucagon secretion ($p < 0.05$, student's t-test, $n = 5$ animals) compared to baseline, while ghrelin and GIP levels remained relatively stable in the response phase. In contrast, control animals exhibited metabolic responses aligned with a fasted state, with an increase in ghrelin and glucagon, and no change in GLP-1, GIP, or insulin. Immunohistochemical staining revealed presence of VGLUT2 and S-100 (markers of vagal afferents) positive cells around the implantation location suggesting the presence of vagal afferents within 100 μm of the implant/tissue interface (Supplemental Figure 9)[54]. To isolate the contribution of mechanical stimulation, as opposed to electrical stimulation, of mechanosensory afferent neurons, the metabolic profile following 30 minutes of passive stretching of the oesophagus with simulated bolus ingestion in 4 animals was analysed (Supplemental Figure 10). Mechanical stimulation alone did not significantly reflect a postprandial metabolic profile. We hypothesize that this may be due to the adaptation rate of stretch receptors in the oesophagus that may be better modulated with electrical stimulation as compared to mechanical stimulation, although this requires further investigation. These findings provide preliminary evidence that gastric and oesophageal neuromodulation by the neuroprosthesis may induce changes in metabolic hormones commensurate with a postprandial state.

Biocompatibility

Previous studies have demonstrated chronic utility of fibre-based neural probes in the brain, spinal cord, and GI lumen of rodents[33,55], as

well as the ability of these devices to support functional skeletal muscle regeneration following volumetric muscle injury in rodents[56]. Here, we further evaluate chronic tissue-material interactions and biocompatibility of the neuroprosthesis containing polycarbonate and stainless steel in vitro and in vivo (Methods). In vitro, an extract exposure test on C2C12 cells demonstrated no significant toxicity at 24 or 168 h as compared to a negative control ($p < 0.05$, student's t-test). In vivo, 7 days following implantation, oesophageal distensibility and dynamics exhibited negligible differences in comparison to pre-implantation measurements (Supplemental Table 3). Complete healing and no substantial foreign body response or migration was observed in stomach and oesophageal tissues (Supplemental Note 1 and Supplemental Figure 11).

Discussion

We demonstrate a closed-loop GI neuroprosthesis that restores peristalsis in models of hyper- and hypomotile pathology. Following sensation of ingested food, the neuroprosthesis delivers electrical and chemical stimulation to generate propagative peristalsis in the oesophagus. As the neuroprosthesis mechanistically recreates peristalsis by recapitulating neuromuscular signalling patterns, the generated movements approximate physiologic contractility, spatial sequence, and efficacy of propelling food boluses in the oesophagus (Fig. 5). Further, in a paretic stomach, electrical stimulation of the submucosal layer in the antrum of the stomach by the neuroprosthesis augments enteric signalling, doubling the motility rate. This is in contrast to the clinical state of the art, wherein point source stimulation is insufficient to generate propagative peristalsis[16,57,58]. Although previous preclinical studies have proposed implanting hardware submucosally, these pilot studies relied on multi-centimetre incisions, focused on unimodal stimulation, and failed to demonstrate electrical stimulation of tissue, or restoration of neuromuscular function[16,59–61].

The neuroprosthesis can be tailored to conform to a specific anatomy and pathology, given its numerous stimulation and sensing contacts and controller design. For instance, in the oesophagus, the proximal third is comprised of striated muscle, whereas the distal third is comprised predominantly of smooth muscle. Based on the anatomic location of implantation, individual electrode parameters in the neuroprosthesis can be programmed to target specific muscle types. The controller's parameters can further be adjusted to modulate the refractory period, magnitude, timing, sequence, and repetition of smooth muscle activation. This versatility offers therapeutic advantages for oesophageal motility disorders like GERD, achalasia, jackhammer oesophagus, absent peristalsis, and upper/ lower oesophageal sphincter dysfunction, which require patient- and disease-specific realignment of neuromuscular activity involving stimulatory and inhibitory modulation.

ENS neuromodulation remains underexplored due to the challenges of interfacing with the deep-set and distributed nature of the enteric plexi. Previously, cervical and gastric vagal stimulation have elicited a variety of responses, with little mechanistic clarity. In the context of using ENS neuromodulation to address eating disorders, our neuroprosthesis' design can be leveraged to recruit intact neural circuitry and simulate the ingestion of a meal and trigger hormonal changes commensurate with a fed state. The metabolic hormone profile following thirty minutes of oesophageal neuromodulation appeared to recapitulate a satiated state, with low glucagon and ghrelin levels (Fig. 6). Because passive mechanical stretching alone did not induce a similar response (Supplemental Figure 10), we anticipate that the stimulation amplitude could be further reduced to elicit minimally perceptible actuation to maximize patient comfort. The insulin response is consistent with food consumption, even in the absence of food in this case[61]. As such, neuromodulation can potentially facilitate perception of satiety, offering therapeutic alternatives for metabolic disorders in which low or late satiety exacerbates energy expenditure imbalances[62,63]. The on-demand production of insulin could also contribute to the understanding and management of type 1 diabetes[64] and other insulin dysregulation conditions.

In this study, all experiments were conducted with the animal in a fasted state in an anaesthesia-induced model of decreased motility. In future experiments, the neuroprosthesis should be chronically evaluated in a fed state in disease models. Additionally, further testing using a wider range of food with varying consistency will refine and validate the ability of the closed-loop system to drive peristalsis. In addition to serving as a therapeutic device, the neuroprosthesis' electrical sensing capabilities may serve a diagnostic purpose as well. Spatially organized electrogastrograms acquired over the course of days would augment our foundational knowledge of motility and metabolism. We utilized glucagon as a proof-of-concept inhibitory neuromodulator to validate neuroprosthetic function. Future formulations will employ combinations of neurotransmitters informed by the evolving understanding of neural circuits governing motility. Additionally, antispasmodic drugs such as baclofen may also be used for inhibition of the smooth muscle.

Future clinical translation of this technology will involve preclinical long-term studies in large animal models to further establish safety and efficacy, to identify disease-specific stimulation parameters, and to refine the surgical techniques. Although this device would offer benefits for motility disorders such as gastroparesis and achalasia, the applications of this technology could further extend to disorders of neurochemical or metabolic signalling, such as diabetes and obesity. Temporal and neuroplastic changes in the brain, as well as habituation to stimulation should be investigated in the future. Varied stimulation paradigms and closed-loop control may present opportunities to overcome potential adaptation responses by the body. In future long-term translational studies, wires from the implant would be tunnelled from the submucosal space to a subcutaneously placed implantable pulse generator akin to those used in commercial neuromodulators and pace-makers (Supplemental Figure 15). As wireless powering systems continue to mature, the wires could be eliminated to permit independent lead-less operation of the prostheses in the submucosal space[65,66]. Polycarbonate, which elicits a minimal foreign body response in neural implants ~ 300um wide[32], was selected for this device to balance the stiffness required for insertion without buckling with biocompatibility. At a diameter of 1.25 mm, the device studied here is likely to elicit a greater foreign body response. While the resulting encapsulation will help with securing the implant in place, it will also lead to decreased recorded signal quality over time. Replacing the polymer cladding with soft and stretchable elastomers such as SEBS (styrene-ethylene-butylene-styrene)[67] will likely further reduce this foreign body response and ensure stable recording and stimulation over time. However, such stretchable systems require further evaluation and optimization. Building on numerous studies demonstrating chronic biocompatibility of polymer fibres in the brain, spinal cord, peripheral musculature, and GI lumen[32–34,56,67], future work should further investigate chronic tissue-material interactions in the submucosal space to ensure long term functionality and safety.

This study was enabled by two key innovations: (1) the multimodal, closed-loop myenteric neuroprosthesis that demonstrates greater conformability and adaptability to GI physiology as compared to existing devices (Supplemental Table 1 and 2) the minimally invasive deployment tool that facilitates submucosal implantation along the GI tract through feedback-driven mucosal plane localization. Notably, in our experiments in the swine model, for which GI anatomy closely resembles that of a human, veterinarian technicians with less than 5 years of experiences or naïve operators (postdoctoral trainees) performed implantation using the implantation tools, without cautery, perforation, or trauma, illustrating the facility of use and safety. Our implantation and neuromodulation platform thus offers an approach to augment the function of the myenteric plexus for motility and

metabolic disorders, that is mechanism-driven, customizable to each patient, and easy-to-implement without specialized training, paving way toward personalized bioelectronic therapies for GI dysfunction.

Methods

All studies were compliant with relevant ethical regulations and under approved protocols by the Massachusetts Institute of Technology. Researchers were not blinded to the interventions, as this was not relevant or feasible in this proof of concept study. Following studies, animals were euthanized under anaesthesia with Telazol and xylazine or midazolam and dexmedetomidine (as outline earlier), then Fatal Plus or Euthosol (sodium pentobarbital) at ~100 mg/kg IV or ~1 ml/10 pounds

Study design

Our objective was to assess the ability of the neuroprosthesis to generate coordinated patterns of motility in the oesophagus and stomach under optimized electrical stimulation patterns. We additionally performed assessments of the surgical complexity of implantation and biocompatibility of the implant. All animal experiments were conducted in accordance with protocols approved by the Committee on Animal Care at the Massachusetts Institute of Technology (MIT). All large animal studies were performed in a swine model (50- to 80-kg Yorkshire pigs ranging between 4 and 6 months of age). The swine model was chosen because its gastric anatomy is similar to that of humans and has been widely used in the evaluation of biomedical GI devices[68]. Before endoscopic procedures and experiments described in this study, animals were fasted overnight. Animals were fed LabDiet mini-pig grower pellets (5081) at 7:30 a.m. and 3:30 p.m. and a snack of fruit or vegetables between 11 a.m. and 12 p.m. Sex was not considered in this study, as gastric and oesophageal peristalsis are not known to vary with sex.

Characterization of peristaltic dynamics & optimization of electrical stimulation parameters

Peristalsis in response to electrical stimulation was studied using both in vivo and ex vivo models. An ex vivo tissue maintenance system was custom-made to characterize contraction dynamics under varying electrical stimulation parameters towards optimizing the dimensions, design, and control algorithm of the implant (Supplemental Figure 12). In a bath of Krebs Ringer solution (Sigma), maintained at 37 °C using an underwater heating element, piping was constructed to enable an inflow and outflow tract for the oesophagus. Measurements of tissue displacement were enabled by centimetre-resolution gridding underneath the tissue and a video camera placed 3 feet above the bath. Tissue from a euthanized pig was transferred to the bath shortly upon harvest after three washes with warm phosphate buffered saline. Bipolar needle electrodes (32 g, Rythmlink) were manually inserted into the intramuscular layer at measured intervals of 1–1.5 cm along with a ground electrode. Electrodes were inserted into serosal, submucosal, or muscularis layer of the oesophagus and the EMG response was captured in response to 40 Hz, 3 ma, 3 s stimulation. The amplitude and strength of contraction were found to be strongest when electrodes were placed in the submucosal layer. Spacing of the electrodes was also varied between 0.5 and 2 cm in 0.5 cm increments and the spatial dynamics of contraction were studied, yielding an optimal spacing of 1 cm between contacts (Supplemental Figure 12). In order to propagate a bolus using ES pulses, we learned that the proximal segment must remain contracted for at least half the duration of the pulse to propagate in the anterograde direction. These insights were used to design the neuroprosthesis and controller.

For in vivo study, standard oval, 2.3 mm × 240 cm length polypectomy snares (Telemed Systems, Inc, MA) were modified with a 25-gauge needle tips to create endoscopic intramuscular electrodes. Two to four electrodes were inserted into tissue in a sequential manner with equal spacing between electrodes (either 1 or 2 cm) in the oesophagus and stomach of swine (n = 5).

A range of stimulation parameters (frequencies: 20, 40, 100 Hz, amplitudes: 1-9 mA in 1 mA increments, pulse widths: 100 or 300 μs, pulse train lengths: 0.5, 1, or 3 s) were programmed into the Synapse system (TDT -Tucker-Davis Technologies) and output onto an IZ2 stimulator (TDT). Electrophysiological recordings were carried out on a Rz5D Base processer and PZ5 neurodigitizer amplifier (TDT) or on a RHS Stimulation/Recording System (Intan Technologies).

Endoscopic video was captured by the Pentax endoscopy suite. The peristaltic rate (number of times the pylorus closed/time, which is known to be proportional to gastric peristalsis)[69] and percent closure of the muscle ring in the oesophagus were used to evaluate and optimize the electrical stimulation parameters. Image analysis was performed semi-manually using functions of Fiji (open source from GitHub). Optimal spacing between contacts and depth of insertion were also evaluated to inform the design of the neuroprosthesis (Supplemental figure 13).

Neuroprosthesis fabrication

The neuroprosthesis consists of a combination of perfluoro alkoxy alkanes (PFA) coated stainless-steel (SS) electrodes, embedded in polycarbonate (PC) housing. The neuroprosthesis was fabricated via thermal drawing of a macroscale model, termed preform. To fabricate the preform, a PC rod (diameter 0.75 in; McMaster-Carr) was first machined to have a central circular channel (diameter 5.5 mm), and eight square grooves (4 × 4 × 200 mm) were machined at the periphery of the rod. Polytetrafluoroethylene (PTFE) rods were used as spacer and were placed inside the central circular channel (7/32 in, PTFE, McMaster-Carr), and peripheral groove (5/32 in, PTFE, McMaster-Carr). PC sheets (50 μm, Ajedium films) were then rolled around the assembly to obtain cylinder with a diameter of 22 mm. The entire structure was then consolidated at 175 °C for 32 min under vacuum. A fibre was then drawn at 270 °C, and the drawing speed was varied from 0.2 to 0.4 mm/min with a feed speed of 1 mm/min to achieve draw-down ratios in the range of 14 to 20. PFA-coated stainless-steel wire (32 G, annealed, A-M systems) was converged into the 8 outer channels of the preform while the device was drawn. Electrode wires from the neuroprosthesis were connectorized to 4 mm header pins (Digikey) using adhesive and flux-solder.

Electrode creation

The Solafab Micromachining Tabletop workstation (Clark MXR) utilizing a Solas Ultrafast Fibre Laser was employed to etch the polymer cladding on the drawn fibres and expose electrodes contacts at the desired spacing (1-1.5 cm), determined through ex vivo peristaltic dynamics characterization (Supplemental Figure 13). The drawn fibre was secured in a custom-made octagonal rotary jig (Supplemental Figure 14) to enable consistent positioning and etch angles for the fibre. Laser power (L20–L100), radius of etch (0.05–0.8 mm), depth (0.1–0.35 mm), length (0.25–1 cm) and pattern (repetition of strokes 1–8 times) were optimized through iterative testing to yield a flat recessed geometry for optimal current injection and contact against wet tissue. Electrode pads were then sonicated for 15 minutes then manually cleaned under a microscope to remove residual debris following the etch. Electrodes were sterilized using ethylene oxide prior to in vivo usage.

Closed-loop electrical stimulation algorithm

A closed-loop control algorithm to perform stimulation in response to a change in impedance or EMG was programmed using MATLAB and the Intan RHX software (beta version, 2020). After the algorithm initializes, it begins recording impedance or EMG on all stimulation

channels. Once a pre-set threshold impedance or rectified EMG is achieved, electrical stimulation is administered. Impedance is measured between a given electrode and the last electrode contact, serving as the ground electrode. The MATLAB controller interfaced with the Intan RHS Recording/Stimulation System via a Transmission Control Protocol (TCP) command interface, allowing stim parameters to be set and data to be recorded remotely (Supplemental Code 1).

Submucosal implantation tool fabrication

The submucosal implantation tool was designed to perform implantation via an endoscopic approach for any devices that need placement in the submucosal space without the invasiveness of a NOTES or POEM technique. The tool was fabricated using a PTFE sheath (McMaster, 2.6 mm diameter). Non-insulated 22-gauge guidewire was coated with a thin layer of silicone (Sylguard 184, Sigma) excluding the 3 cm from distal tip to serve as the impedance sensing unit. Nitinol (28-gauge, Fort Wayne Metals, #8) was set in a custom vice at 400 °C for 3 minutes and quenched in water at 25 °C to create a hook. The distal tip was bevelled using a Dremel at an angle of 45 degrees. Following fabrication, the entire device was loaded with sterile saline and all sliding parts were articulated at least 3 times prior to use. 50 mL syringes were pre-loaded with diluted methylene blue solutions in sterile saline and connected to a syringe coupler.

Implantation procedure with submucosal implantation tool

For use, the pre-loaded 1.9 cm diameter sheath is inserted through the endoscopic channel and advanced to the proximal site of implant. The incision catheter is advanced while holding the overtube in place relative to the endoscope, facilitated by an O-ring stabilizer. A nitinol hook is deployed in the adjacent channel to hold tension on the site of incision. The incision catheter is advanced while continually monitoring impedance to detect localization in the submucosal layer (<100kOhms, Fig. 2). Hydrodissection is then performed with 10-35 mL saline while monitoring the expansion of the layer intraluminally via endoscopic video. The guide wire is then advanced to a length commensurate with the prosthesis to ensure clear separation of the fascial layer in the path into which the prosthesis will glide. The guide wire is removed, and the prosthesis is inserted. Fibrin glue may be infused through the microfluidic channel or a Carr-Locke/endoscopy needle to secure the end of the prosthesis in the tissue layer. Leads can then be tunnelled out to a subcutaneous pocket or through a PEG tube to a stimulator.

Rationale for design of incising needle

A variety of designs were created to optimize the needle edge for penetration of the oesophagus at low force without high perforation risk. The angling of an endoscope creates, at best, a 20-degree angle between the catheter and the tissue. Thus, the following designs were tried given the relevant rationale from prior studies[70].

The triple grooved tip and pitchfork tip were developed with the aim of catching the tissue that glides within the grooves, creating a wedge scissoring effect.

The curved tip was developed to implement the slide-push effect during penetration, which is known to cause a reduction in cutting forces and displacement of the medium.

The broad base needle tip was designed with a reduced bevel angle to increase the angle of attack of the cutting surface on the tissue, reducing the chance of slip during the incision.

The dual point design was intended to allow for a cutting edge to be in contact with the tissue regardless of twist angle, as it is difficult to adjust the twist of the tip once in the endoscope.

These were all compared against standard bevel designs to evaluate their force requirement upon penetration of the compliant GI tissues.

Incisional needle testing

Various designs for the incising needle tip were designed in SolidWorks (Supplemental Fig. 5). Mechanical tools including wire cutters, Dremel, band saw, drill press, and metal sharpeners were used to fabricate the various designs. Needle tips were pneumatically secured to the descending plate of the Instron. Ex vivo swine oesophagus and stomach tissue were held in place by vice grips forming a semi-taut interface at either 20° or 90° with respect to the axis of the needle. Force and displacement during incision were measured under a compression mode test (Bluehill Universal) which advanced the needle at 100 mm/minute.

Testing of submucosal implantation tool functionality

To validate the safety and efficacy of the tool, implantations were performed in swine post-euthanasia or harvested oesophagus and stomach ($n = 5$) to ensure that the tool enabled 1) incision of the mucosal layer, 2) accurate localization in the submucosal layer and 3) hydrodissection to mechanically separate the submucosal layer and 4) no perforation of the muscular layer. During implantation, we performed endoscopic videography to visualize the process and assess the difficulty of use. Impedance was measured during the localization process using the Intan RHS Recording/Stimulation System. Following implantation, tissue cross-section was inspected for tissue damage, localization, and separation of layers. We fixed the tissue using 4% paraformaldehyde, marking the incision site with tissue marking dye (Cancer Diagnostics) and performed histology to identify whether the stated objectives were met.

Pressure sensing

To characterize the pressure sensing capabilities of the neuroprosthesis, impedance from the two most proximal electrodes were monitored at 500, 1000, and 2000 Hz. Tissue in which the neuroprosthesis was implanted was explanted and placed on the Instron compression testing system, which performed controlled indentations sweeping from 0-7 N, covering the range of pressures exerted by boluses of food on the equivalent surface area. Between each indentation, 0 N of force were applied for 1 minute to allow the tissue to equilibrate to resting conditions.

Mechanical and Electrochemical characterization of stimulating electrodes

Electrical impedance spectroscopy (EIS) of the stimulating electrodes was measured using a LCR metre (HP4284A, Agilent Technologies) with a sinusoidal voltage input (10 mV, 20 Hz – 10 kHz). A three-electrode cell with a platinum wire as a counter electrode and a saturated Ag/AgCl reference electrode was used to perform cyclic voltammetry (CV). CV was performed in phosphate-buffered saline solution, at room temperature, using a potentiostat (Solartron, SI 1280B), and cyclic voltammetry curves were obtained at the scan rate of 20 mV/s. Charge-injection capacities were determined from voltage transient measurements in response to cathodic-first, rectangular charge-balanced biphasic pulses (100 µs, 0.5 mA to 10 mA) with a 33.3 µs interphase delay between cathodic and anodic phases using an Intan RHS Recording/Stimulation System and an oscilloscope. The maximum cathodic potential E_{mc} was measured during the interphase interval, near-instantaneously following the ohmic voltage drop in the electrolyte (access voltage–V_a)[36]. Accelerated aging test consisted of prolonged current stimulation pattern (4 mA, charge balanced biphasic rectangular pulses of half-phase period 100 µs) in a 1× PBS solution using constant current stimulators NL800A (Digitimer) for 24 h. Every 30 min to 1 h, voltage transient responses to a cathodic first biphasic stimulation with interphase delay was used to measure the E_{mc} and estimate charge injection capacity.

Cyclic buckling of the neuroprosthesis was performed via a custom set-up composed of linear stage actuated by a stepper motor,

described previously[71]. For all samples, the neuroprosthesis was compressed then relaxed at a speed of 1 cm/sec, with a displacement of 5 mm. Bending stiffness of the fibres ($n = 3$) was measured using a dynamical mechanical analyser (Q800, TA Instruments). A single cantilever mode with 20 μm deformation was used within the frequency range of 0.1–200 Hz.

Tensile testing of the fibres was performed at a rate of 10 mm min^{-1} using a Zwick/Roell Z2.5 mechanical tester. The nominal stress S was measured from the recorded force divided by the cross-sectional area of the fibre, and the Young's modulus was derived from the slope of the stress-strain curve in the elastic regime. Three-point bending testing of the neuroprosthesis was performed at a rate of 60 mm/min, with a maximum displacement of 20 mm, using a Zwick/Roell Z2.5 mechanical tester. The neuroprosthesis was supported at two points 30 mm apart. The bending stiffness m was derived from the slope of the linear part of the force-deflection curve. The relation between the bending stiffness and the flexural strength is given by

$$m = \frac{48 E_f I}{L^3}$$

with I being the inertia moment of a cylindrical beam, E_f the flexural modulus, and L the support span. Knowing the inertia moment of a cylindrical beam

$$I = \frac{\pi R^4}{4}$$

Where R is the radius of the fibre. We thus obtain an expression for the flexural modulus:

$$E_f = \frac{mL^3}{12\pi r^4}$$

In vitro assessment of biocompatibility

We performed an extract exposure test[72] following ISO norms to evaluate the toxicity of the neuroprosthesis material. 0.2 g of material were added to 1 mL of DMEM culture medium and stirred at 37 °C continuously for 24 h and 168 h (7 days)days to create the extract samples. 100 μL of foetal bovine serum were added to 900 μL aliquots of the samples and used to treat C2C12 cells[73] plated in a 96 well plate in triplicate. These cells tested negative for mycoplasma. A negative control of untreated media and positive control of media containing 40 μm MG-132, a small molecule proteasome inhibitor, were also performed. At 24 and 72 h, cell viability was measured through quantitation of ATP using CellTiter-Glo (Promega) using a Tecan M1000Pro.

In vivo assessment of biocompatibility

Rats ($n = 14$, weighing between 300 and 350 g, Charles River Laboratories) were anesthetized with 1 to 2% isoflurane in oxygen and premedicated with meloxicam (1 mg/ kg). A small incision was made in the skin of the lateral abdomen and blunt dissection was performed to create a small subcutaneous pocket where a 1.5 cm segment of the polycarbonate and stainless-steel device was implanted. At 2- and 4-weeks post implantation, 7 animals each were euthanized and the tissue surrounding the implant was harvested and fixed in 4% paraformaldehyde.

Female Yorkshire swine from Cummings Veterinary School at Tufts University (Grafton, MA) between 30-40 kg were anesthetized with an intramuscular injection of dexmedetomidine (0.03 mg/kg) and midazolam (0.25 mg/kg) and intubated and maintained on 2-3% isoflurane in oxygen. A 15 cm fibre was implanted in the submucosal space in the middle oesophagus and stomach using the minimally-invasive tool. One resolution clip (235 cm, 2.8 mm, Boston Scientific) was placed to close the incision site. No haematologic or infectious complications occurred. Seven days later, the area was examined endoscopically to find no gross complications or swelling. The oesophagus was excised and fixed in 4% formalin for histologic evaluation.

Following fixation, samples were washed with phosphate buffered saline (Sigma), transferred to 70% ethanol, paraffin processed and embedded. Five micron-thick sections were cut every 100 μm and stained with haematoxylin and eosin.

Ex vivo assessment of functionality following a month-long implantation

To highlight the capability of the neuroprosthesis to be used in an acute setting following a month-long-implantation, a 15 cm fibre was implanted in the submucosal space in the middle oesophagus using the minimally invasive tool of anesthetized Female Yorkshire swine (N = 2) (similar method as described above). A month following implantation, the animals were euthanized, the oesophagus was excised, and placed into a bath of Belzer solution to maximize viability. The connector of the neuroprosthesis was exposed and the electrode leads were connected to our stimulating apparatus (Intan RHX). Following initial testing of tissue viability using a CheckPoint Surgical Stimulator, the tissue was stimulated using the neuroprosthesis' electrodes, and muscular contraction of the oesophagus was video recorded. Finally, oesophageal tissues were fixed in 4% PFA, and histological sections were taken and stained with haematoxylin and eosin, showing little to no scarring around the location of the implant.

Artificial peristalsis

Following validation of the safety, efficacy, and biocompatibility, the prosthesis was implanted Yorkshire swine (n = 2, 94 kg & 70 kg). The optimized electrical stimulation parameters were programmed into the controller. A pump primed the microfluidic channel and injected 5 mg/mL glucagon per neurochemical stimulus.

As a well-known model for temporarily-induced dysmotility, isoflurane anaesthesia affects muscarinic receptors (TRPC4 channels, M2 and M3) and smooth muscle G-proteins[74] as a function of concentration[75] and anaesthetic period. We used the following procedure to induce temporary dysmotility. Under 2-2.5% inhaled isoflurane anaesthesia, at least three laryngeal strokes using a small PTFE tube were performed and monitored through endoscopy and/or intraluminal functional imaging to reveal no swallow reflex. Then, barium impregnated pellets were placed in the upper, middle, and lower oesophagus and monitored fluoroscopically for 10 minutes each, revealing no movement. After 1 h of anaesthesia, gastric motility was depressed as evidenced by a lowered rate of peristaltic movement. As such, titrated anaesthesia concentration and duration provided a suitable model for complete oesophageal dysmotility and depressed gastric motility.

To characterize and validate the neuroprosthesis' ability to sense and create artificial peristalsis, a fluoroscopic pellet study was conducted. Barium sulphate (Bracco E-Z-HD Barium Sulphate for Suspension (98%w/w), Patterson Veterinary) was mixed with a sodium alginate solution (Sigma) in a 50:50 volume by weight ratio. After 10 minutes of sonication at 30 °C, the suspension was pipetted into a custom silicone mould sized for a triple zero capsule. After 24 h, these pellets were hydrated with a 2 M CaCl2 solution for at least 2 h and rinsed with PBS for 72 h. They were then placed in the oesophagus using the endoscope. Stimulation and sensing were performed by the neuroprosthesis and the pellet was radiographically visualized using fluoroscopy. Further, intraluminal functional imaging studies were performed ($n = 4$, swine) to characterize changes in oesophageal reflexes and pressures following tool-based tissue manipulation and neuroprosthesis implantation as well as capture artificial peristalsis created by the neuroprosthesis. A functional lumen imaging probe (Endoflip, Medtronic) was inserted into the middle and lower oesophagus using an overtube to profile distensibility,

pressure, pattern of motility and minimal diameter of the oesophagus. Data was exported and visualized using plotting functions in Matlab. Electromyography was recorded from the electrodes during stimulation and rest periods. Data were imported and low-pass filtered to identify slow wave activity in the stomach.

Neuromodulation

Beyond effects on motility, neuromodulatory effects on metabolic processes was assayed by screening the blood of Yorkshire swine receiving 30 minutes of oesophageal muscular stimulation ($n = 6$) or no stimulation, under sedation (n = 6). A metabolic hormone panel (Eve Technologies) was run on venous blood from an ear vein catheter, collected 30 minutes prior to stimulation and every 30 minutes for 2 h. Blood was treated with a protease inhibitor cocktail (S8830, Sigma) within 10 minutes of collection and centrifuged for 15 minutes at 4 °C at 700 g's. Results were normalized to the baseline values at t = 0 min or the average of the two time points prior to stimulation (t = 0, 15)

To ascertain whether the effects of oesophageal stimulation by the neuroprosthesis are modulated by mechanotransducers perceiving the contractions or electrical stimulation directly triggering the related afferents, we performed an experiment in which mechanotransducers in the oesophagus were passively stretched. For 30 minutes, a bolus situated on a catheter was slid up and down the oesophagus to mimic the ingestion of food. The bolus consisted of 40 mL of saline in a 4.5 cm balloon catheter at least doubling the resting diameter of the oesophagus. A metabolic hormone panel was performed on blood collected from an ear vein catheter as described above.

Statistical analyses

Quantitative data are reported as mean ± standard deviation or as a range when appropriate. The normality of the distributions was checked by the Shapiro-Wilk test. Comparative analyses were performed using student's heteroscedastic two-tailed t-test, unless otherwise noted. $P < 0.05$ was considered significant. Unless otherwise noted, measurements were performed on independent samples (animals or tissue sections).

Supplemental note 1: assessment of biocompatibility. An extract exposure test on C2C12 cells demonstrated no significant difference in toxicity between the negative control and the neuroprosthesis material at 24 and 168 h (Supplemental Figure 11a), while 40 µM of toxic MG-132 treatment, used as positive control, resulted in significantly decreased cell viability ($p < 0.05$, student's t-test). Following seven days of implantation in a swine oesophagus, functional lumen imaging was performed to elicit the swallowing reflex, which occurred naturally at inflations greater than 20 mL. Compared to the baseline prior to implantation, we observed minimal differences in the distensibility and CSA_{min} of the oesophagus, indicating the negligible impact of the prosthesis on organ dynamics (Supplemental Table 3). Further, no significant foreign body reactions, scarring or migration were observed (Supplemental Figure 11b). Finally, we confirmed accurate placement of the prosthesis in the submucosal layer, adjoining the circular muscle (Supplemental Figure 11b, inset). Haematoxylin and eosin staining of subcutaneous tissues implanted with the neuroprosthesis for 14 and 28 days demonstrated a thin collagenous fibrous capsule forming around the material (Supplemental Figure 11e), but no substantial foreign body response (Supplemental Figure 11C) as compared to non-implanted control sections (Supplemental Figure 11d, f). This type of a capsule is common to all intramuscular electrodes and does not present a significant issue for stimulation[76]. Similar types of electrodes are clinically-approved for use in human patients and are routinely employed by for myoelectric recording and stimulation. Furthermore, as the stimulation is current driven, the backend compliance of our system enables consistent current output, regardless of the impedance at the surface and can stimulate the tissue consistently, even if the fibrous capsule were to increase the impedance of the system, provided the voltage required doesn't exceed the water window of our electrodes. During endoscopy and following explanation of the neuroprosthesis, the oesophageal mucosa and lamina propria at the incision site demonstrated full healing with anticipated fibrosis (Supplemental Figure 11g). Submucosal collagen was found to be slightly separated and cushioning the implant as compared to a control segment of the stomach, although no adverse biocompatibility concerns were seen (Supplemental Figure 11h).

Poly(carbonate) used as the outer cladding of our neuroprosthesis is considered a biocompatible material and has been utilized in several FDA-approved medical products ranging from surgical instruments and IV connection components to cardiac surgery products and renal dialysis–cases in which blood and other bodily tissues are in direct contact. Further, poly(carbonate) grades are available that comply with biocompatibility testing standards such as ISO 10993-1 and USP Class VI. Thus, we do not anticipate any significant biocompatibility concerns. Additionally, given versatility of thermal drawing the cladding material of poly(carbonate) can in future be easily replaced by other materials in the translational phases of this project.

Reporting summary

Further information on research design is available in the Nature Portfolio Reporting Summary linked to this article.

Data availability

Source data are provided with this paper. The raw data are available for research purposes from the corresponding authors on request. All data associated with this study are presented in the manuscript or the Supplemental Materials.

Code availability

The code utilized in this study is available in the supplementary materials, and at this hyperlink https://zenodo.org/records/13338548.

References

1. Huizinga, J. D. & Lammers, W. J. E. P. Gut peristalsis is governed by a multitude of cooperating mechanisms. *Am. J. Physiol. -Gastrointest. Liver Physiol.* **296**, G1–G8 (2009).
2. Chen, J. D. Z., Yin, J. & Wei, W. Electrical therapies for gastrointestinal motility disorders. *Expert Rev. Gastroenterol. Amp Hepatol.* **11**, 407–418 (2017).
3. Yu, D. et al. The burdens, concerns, and quality of life of patients with gastroparesis. *Dig. Dis. Sci.* **62**, 879–893 (2017).
4. Aguilera-Lizarraga, J. et al. Local immune response to food antigens drives meal-induced abdominal pain. *Nature* **590**, 151–156 (2021).
5. Camilleri, M. Gastrointestinal motility disorders in neurologic disease. *J. Clin. Invest.* **131**, e143771 (2021).
6. Park, S. K. et al. Changes in pressure waves after endoscopic intervention in patients with achalasia: A focus on peristaltic recovery of the esophageal body. *Turk. J. Gastroenterol.* **27**, 4–9 (2016).
7. Roman, S. et al. Partial Recovery of Peristalsis After Myotomy for Achalasia. *JAMA Surg.* **148**, 157 (2013).
8. Greenberger, N., Blumberg, R. & Burakoff, R. *CURRENT Diagnosis & Treatment Gastroenterology, Hepatology, & Endoscopy, Third Edition*. (McGraw-Hill Education / Medical, 2015).
9. Powley, T. L. et al. Architecture of vagal motor units controlling striated muscle of esophagus: Peripheral elements patterning peristalsis?. *Auton. Neurosci.* **179**, 90–98 (2013).
10. Travagli, R. A. & Anselmi, L. Vagal neurocircuitry and its influence on gastric motility. *Nat. Rev. Gastroenterol. Amp Hepatol.* **13**, 389–401 (2016).
11. Rogers, R. C., Hermann, G. E. & Travagli, R. A. Brainstem pathways responsible for oesophageal control of gastric motility and tone in the rat. *J. Physiol.* **514**, 369–383 (1999).

12. Berthoud, H. -r. Vagal and hormonal gut–brain communication: from satiation to satisfaction. *Neurogastroenterol. Amp Motil.* **20**, 64–72 (2008).
13. Janssen, P. et al. Review article: the role of gastric motility in the control of food intake. *Aliment. Pharmacol. Amp Ther.* **33**, 880–894 (2011).
14. Cummings, D. E. & Overduin, J. Gastrointestinal regulation of food intake. *J. Clin. Invest.* **117**, 13–23 (2007).
15. Pasricha, P. J. Hunger games: is your stomach making you fat?. *Gastroenterology* **148**, 491–493 (2015).
16. Ramadi, K. B., Srinivasan, S. S. & Traverso, G. Electroceuticals in the gastrointestinal tract. *Trends Pharmacol. Sci.* **41**, 960–976 (2020).
17. Bilgutay, A. M., Wingrove, R., Griffen, W. O., Bonnabeau, R. C. & Lillehei, C. W. Gastro-intestinal Pacing A New Concept in the Treatment of Ileus. *Ann. Surg.* **158**, 338–347 (1963).
18. Soffer, E. E. Gastric electrical stimulation for gastroparesis. *J. Neurogastroenterol. Motil.* **18**, 131–137 (2012).
19. Ducrotte, P. et al. Gastric electrical stimulation reduces refractory vomiting in a randomized crossover trial. *Gastroenterology* **158**, 506–514.e2 (2020).
20. Zoll, B. et al. Gastric electric stimulation for refractory gastroparesis. *J. Clin. Outcomes Manag. JCOM* **26**, 27–38 (2019).
21. Bielefeldt, K. Adverse events of gastric electrical stimulators recorded in the Manufacturer and User Device Experience (MAUDE) Registry. *Auton. Neurosci.* **202**, 40–44 (2017).
22. Paterson, W. G. et al. Esophageal peristalsis. *GI Motil. Online* https://doi.org/10.1038/gimo13 (2006).
23. Payne, S. C., Furness, J. B. & Stebbing, M. J. Bioelectric neuromodulation for gastrointestinal disorders: effectiveness and mechanisms. *Nat. Rev. Gastroenterol. Amp Hepatol.* **16**, 89–105 (2018).
24. Lo, Y.-K. et al. A wireless implant for gastrointestinal motility disorders. *Micromachines* **9**, 17 (2018).
25. Sevcencu, C., Rijkhoff, N. J. M. & Sinkjaer, T. Colon emptying induced by sequential electrical stimulation in rats. *IEEE Trans. Neural Syst. Rehabil. Eng.* **13**, 516–523 (2005).
26. Xing, J. H., Lei, Y. & Chen, J. D. Z. Gastric Electrical Stimulation (GES) with Parameters for Morbid Obesity Elevates Lower Esophageal Sphincter (LES) Pressure in Conscious Dogs. *Obes. Surg.* **15**, 1321–1327 (2005).
27. Rodríguez, L. et al. Long-term results of electrical stimulation of the lower esophageal sphincter for the treatment of gastroesophageal reflux disease. *Endoscopy* **45**, 595–604 (2013).
28. Desilets, D. NOTES: alive and well. *Gastrointest. Endosc.* **89**, 878–879 (2019).
29. Kurniawan, N. & Keuchel, M. Flexible gastro-intestinal endoscopy — clinical challenges and technical achievements. *Comput. Struct. Biotechnol. J.* **15**, 168–179 (2017).
30. Rao, S. S. C., Lee, Y. Y. & Ghoshal, U. C. *Clinical and Basic Neurogastroenterology and Motility*. (Elsevier Science & Technology, 2019).
31. Gunaydin, L. A. et al. Natural neural projection dynamics underlying social behavior. *Cell* **157**, 1535–1551 (2014).
32. Antonini, M. et al. Customizing MRI-compatible multifunctional neural interfaces through fiber drawing. *Adv. Funct. Mater.* **31**, 2104857 (2021).
33. Canales, A. et al. Multifunctional fibers for simultaneous optical, electrical and chemical interrogation of neural circuits in vivo. *Nat. Biotechnol.* **33**, 277–284 (2015).
34. Park, S. et al. One-step optogenetics with multifunctional flexible polymer fibers. *Nat. Neurosci.* **20**, 612–619 (2017).
35. Schiavone, G. et al. Guidelines to study and develop soft electrode systems for neural stimulation. *Neuron* **108**, 238–258 (2020).
36. Cogan, S. F. Neural stimulation and recording electrodes. *Annu. Rev. Biomed. Eng.* **10**, 275–309 (2008).
37. Boehler, C., Carli, S., Fadiga, L., Stieglitz, T. & Asplund, M. Tutorial: guidelines for standardized performance tests for electrodes intended for neural interfaces and bioelectronics. *Nat. Protoc.* **15**, 3557–3578 (2020).
38. Tanaka, N. et al. Development of a swallowing frequency meter using a laryngeal microphone. *J. Oral. Rehabil.* **39**, 411–420 (2012).
39. Ertekin, C. Voluntary versus spontaneous swallowing in man. *Dysphagia* **26**, 183–192 (2010).
40. Krauss, J. K. et al. Technology of deep brain stimulation: current status and future directions. *Nat. Rev. Neurol.* **17**, 75–87 (2020).
41. Seyock, S., Maybeck, V. & Offenhäusser, A. How to image cell adhesion on soft polymers?. *Micron* **92**, 39–42 (2017).
42. Kay, M. & Wyllie, R. *61 - Esophagogastroduodenoscopy and Related Techniques*. in *Pediatric Gastrointestinal and Liver Disease* (eds. Wyllie, R. & Hyams, J. S.) 626-649 3 (W.B. Saunders, Saint Louis, 2011).
43. Jushiddi, M. G. et al. Bevel angle study of flexible hollow needle insertion into biological mimetic soft-gel: Simulation and experimental validation. *J. Mech. Behav. Biomed. Mater.* **111**, 103896 (2020).
44. Maiss, J., Zopf, Y. & Hahn, E. G. Entrance barriers and integration obstacles of NOTES. *Minim. Invasive Ther. Amp Allied Technol.* **19**, 287–291 (2010).
45. Kahrilas, P. J. & Sifrim, D. High-resolution manometry and impedance-pH/manometry: valuable tools in clinical and investigational esophagology. *Gastroenterology* **135**, 756–769 (2008).
46. Ishida, S., Miyagawa, T., O'Grady, G., Cheng, L. K. & Imai, Y. Quantification of gastric emptying caused by impaired coordination of pyloric closure with antral contraction: a simulation study. *J. R. Soc. Interface* **16**, 20190266 (2019).
47. Ehrlein, H. J. Motility of the pyloric sphincter studied by the inductograph method in conscious dogs. *Am. J. Physiol. -Gastrointest. Liver Physiol.* **254**, G650–G657 (1988).
48. Wang, G., Filip, D., Poscente, M. D., Andrews, C. N. & Mintchev, M. P. *Capsule-Based Measurements of Gastrointestinal Impedance*. in *Handbook of Biochips: Integrated Circuits and Systems for Biology and Medicine* (ed. Sawan, M.) 785–802 (Springer, New York, NY, 2022).
49. Imam, H., Sanmiguel, C., Larive, B., Bhat, Y. & Soffer, E. Study of intestinal flow by combined videofluoroscopy, manometry, and multiple intraluminal impedance. *Am. J. Physiol. -Gastrointest. Liver Physiol.* **286**, G263–G270 (2004).
50. Wilson, J. E. & Fontanarosa, P. B. *Glucagon for the treatment of respiratory emergencies*. in *Glucagon in Acute Medicine: Pharmacological, clinical and therapeutic implications* (ed. Picazo, J.) 27–36 (Springer Netherlands, Dordrecht, 1993).
51. Srinivasan, S. S., Maimon, B. E., Diaz, M., Song, H. & Herr, H. M. Closed-loop functional optogenetic stimulation. *Nat. Commun.* **9**, 5303 (2018).
52. Myers, M. G. & Olson, D. P. SnapShot: neural pathways that control feeding. *Cell Metab.* **19**, 732–732.e1 (2014).
53. Coll, A. P., Farooqi, I. S. & O'Rahilly, S. The hormonal control of food intake. *Cell* **129**, 251–262 (2007).
54. Raab, M. & Neuhuber, W. L. Number and distribution of intraganglionic laminar endings in the mouse esophagus as demonstrated with two different immunohistochemical markers. *J. Histochem. Amp Cytochem.* **53**, 1023–1031 (2005).
55. Lu, C. et al. Flexible and stretchable nanowire-coated fibers for optoelectronic probing of spinal cord circuits. *Sci. Adv.* **3**, e1600955 (2017).
56. Jin, Y. et al. Functional skeletal muscle regeneration with thermally drawn porous fibers and reprogrammed muscle progenitors for volumetric muscle injury. *Adv. Mater.* **33**, e2007946 (2021).
57. Khajanchee, Y. S. et al. Electrical stimulation of the vagus nerve restores motility in an animal model of achalasia. *J. Gastrointest. Surg.* **7**, 843–849 (2003).

58. Lal, N., Livemore, S., Dunne, D. & Khan, I. Gastric electrical stimulation with the Enterra system: a systematic review. *Gastroenterol. Res. Pract.* **2015**, 1–9 (2015).
59. Hajer, J., Novák, M. & Rosina, J. Wirelessly powered endoscopically implantable devices into the Submucosa as the possible treatment of gastroesophageal reflux disease. *Gastroenterol. Res. Pract.* **2019**, 1–7 (2019).
60. Hajer, J. & Novák, M. Development of an autonomous endoscopically implantable submucosal microdevice capable of neurostimulation in the gastrointestinal tract. *Gastroenterol. Res. Pract.* **2017**, 1–8 (2017).
61. Adamska, E. et al. Intake of meals containing high levels of carbohydrates or high levels of unsaturated fatty acids induces postprandial dysmetabolism in young overweight/obese men. *BioMed. Res. Int.* **2015**, 1–9 (2015).
62. Ball, S. D. et al. Prolongation of satiety after low versus moderately high glycemic index meals in obese adolescents. *Pediatrics* **111**, 488–494 (2003).
63. Dalton, M., Hollingworth, S., Blundell, J. & Finlayson, G. Weak satiety responsiveness is a reliable trait associated with hedonic risk factors for overeating among women. *Nutrients* **7**, 7421–7436 (2015).
64. Wilcox, G. Insulin and insulin resistance. *Clin. Biochem. Rev.* **26**, 19–39 (2005).
65. Reddy, V. Y. et al. Percutaneous implantation of an entirely intracardiac leadless pacemaker. *N. Engl. J. Med.* **373**, 1125–1135 (2015).
66. Reynolds, D. et al. A leadless intracardiac transcatheter pacing system. *N. Engl. J. Med.* **374**, 533–541 (2016).
67. Sahasrabudhe, A. et al. Multifunctional microelectronic fibers enable wireless modulation of gut and brain neural circuits. *Nat. Biotechnol.* **42**, 892–904 (2023).
68. Stamatopoulos, K., O'Farrell, C., Simmons, M. & Batchelor, H. In vivo models to evaluate ingestible devices: Present status and current trends. *Adv. Drug Deliv. Rev.* **177**, 113915 (2021).
69. Tse, G., Lai, E. T. H., Yeo, J. M., Tse, V. & Wong, S. H. Mechanisms of Electrical Activation and Conduction in the Gastrointestinal System: Lessons from Cardiac Electrophysiology. *Front. Physiol.* **7**, 182 (2016).
70. Herrera-Granados, G. et al. Effect of cutting angles during the microgroove fabrication process using a non-rigid cutting mechanism. https://conf.papercept.net/images/temp/IWMF/media/files/0017.pdf (2014).
71. Marion, J. S. et al. Thermally drawn highly conductive fibers with controlled elasticity. *Adv. Mater.* **34**, e2201081 (2022).
72. Srivastava, G. K. et al. Comparison between direct contact and extract exposure methods for PFO cytotoxicity evaluation. *Sci. Rep.* **8**, 1425 (2018).
73. Ikeda, K. et al. In vitro drug testing based on contractile activity of C2C12 cells in an epigenetic drug model. *Sci. Rep.* **7**, 44570 (2017).
74. Dryn, D., Luo, J., Melnyk, M., Zholos, A. & Hu, H. Inhalation anaesthetic isoflurane inhibits the muscarinic cation current and carbachol-induced gastrointestinal smooth muscle contractions. *Eur. J. Pharmacol.* **820**, 39–44 (2018).
75. Anderson, D. L. et al. Liquid gastric emptying in the pig: effect of concentration of inhaled isoflurane. *J. Nucl. Med. Publ. Soc. Nucl. Med.* **43**, 968–971 (2002).
76. Memberg, W. D. et al. Implanted neuroprosthesis for restoring arm and hand function in people with high level tetraplegia. *Arch. Phys. Med. Rehabil.* **95**, 1201–1211.e1 (2014).

Acknowledgements

We thank Dr. Walter Chan and Dr.H.A. for consultation on clinical motility diagnosis and treatment. We thank Dr. S.L. for consultation on mechanical characterization of the neuroprosthesis. We thank Virginia Fulford for original artwork included in Fig. 1. This work was funded in part by a grant from the National Institutes of Health (R01EB000244), a grant from N.N., the K.v.T. (1925) Career Development Professorship and the Department of Mechanical Engineering at MIT. S.S.S. is funded by the Schmidt Science Fellows programme. P.A. acknowledges support from the National Institute for Neurological Disorders and Stroke (1R01NS115025-01), National Science Foundation Centre for Neurotechnology (EEC-1028725), the McGovern Institute for Brain Research, and the K. Lisa Yang Brain-Body Centre at MIT.

Author contributions

S.S.S. and M.J.A. conceptualized the GI neuroprosthesis, performed the surgeries, data collection, analysis and writing of the manuscript. A.A., A.S., J.J., K.I., and J.K. assisted with data collection. A.H. oversaw in vivo work. S.M. assisted with fabrication and ex vivo work. R.L., P.A., and G.T. contributed to conceptualization, provided project management, contributed to the experimental design and manuscript preparations.

Competing interests

Shriya Srinivasan, Marc-Joseph Antonini, Polina Anikeeva, Robert Langer, and Giovanni Traverso are co-inventors on provisional patent applications describing the developments presented here. R.L. and G.T. Report receiving consulting fees from Novo Nordisk. Complete details of all relationships for profit and not for profit for G.T. and R.L can be found at as supplemental attachments. All authors have submitted an invention disclosure to MIT. M.-J.A. and P.A. are cofounders of NeuroBionics Inc. that seeks to translate fibre-based technology to treatment of neurological conditions.

Additional information

Supplementary information The online version contains supplementary material available at https://doi.org/10.1038/s41467-025-62413-6.

Correspondence and requests for materials should be addressed to Polina Anikeeva or Giovanni Traverso.

Peer review information *Nature Communications* thanks Marco Capogrosso, Florian Fallegger and the other anonymous reviewer(s) for their contribution to the peer review of this work. A peer review file is available.